Bioactive Materials 6 (2021) 2120–2133

Contents lists available at ScienceDirect

Bioactive Materials

journal homepage: www.sciencedirect.com/journal/bioactive-materials

Fast photocurable thiol-ene elastomers with tunable biodegradability, mechanical and surface properties enhance myoblast differentiation and contractile function

Mohamed Alaa Mohamed [a,b], Aref Shahini [a], Nika Rajabian [a], Julia Caserto [a], Ahmed M. A. El-Sokkary [b], Magda A. Akl [b], Stelios T. Andreadis [a,c,d,*], Chong Cheng [a,**]

[a] Department of Chemical and Biological Engineering, University at Buffalo, The State University of New York, Buffalo, NY, 14260, USA
[b] Chemistry Department, College of Science, Mansoura University, Mansoura, 35516, Egypt
[c] Department of Biomedical Engineering, University at Buffalo, The State University of New York, Buffalo, NY, 14260, USA
[d] Center of Excellence in Bioinformatics and Life Sciences, Buffalo, NY, 14263, USA

ARTICLE INFO

Keywords:
Biodegradable elastomers
Cell culture substrate
Skeletal muscle regeneration
Thiol-ene synthesis
Tissue engineering

ABSTRACT

Biodegradable elastomers are important emerging biomaterials for biomedical applications, particularly in the area of soft-tissue engineering in which scaffolds need to match the physicochemical properties of native tissues. Here, we report novel fast photocurable elastomers with readily tunable mechanical properties, surface wettability, and degradability. These elastomers are prepared by a 5-min UV-irradiation of thiol-ene reaction systems of glycerol tripentenoate (GTP; a triene) or the combination of GTP and 4-pentenyl 4-pentenoate (PP; a diene) with a carefully chosen series of di- or tri-thiols. In the subsequent application study, these elastomers were found to be capable of overcoming delamination of myotubes, a technical bottleneck limiting the *in vitro* growth of mature functional myofibers. The glycerol-based elastomers supported the proliferation of mouse and human myoblasts, as well as myogenic differentiation into contractile myotubes. More notably, while beating mouse myotubes detached from conventional tissue culture plates, they remain adherent on the elastomer surface. The results suggest that these elastomers as novel biomaterials may provide a promising platform for engineering functional soft tissues with potential applications in regenerative medicine or pharmacological testing.

1. Introduction

Skeletal muscle is vital for generating the force necessary for movements and accounts for approximately 45% of the total body mass of human adults [1,2]. Although skeletal muscle has the inherent self-repairing capability, its regeneration is significantly impaired by aging as well as severe traumatic injuries, diseases, myopathies, and cachexia [3]. Tissue engineering has emerged as a powerful strategy for the regeneration of muscle tissue [4–9]. However, early detachment of myotubes from culture substrates, especially after they start beating, hampers the formation of mature muscle tissues. Biodegradable elastomers have shown significant promise for the engineering of soft tissues, such as skeletal muscle, blood vessels, and cartilage [10–15]. In principle, it is critical to design biodegradable elastomers to possess mechanical and surface properties that mimic these soft tissues, in order to achieve scaffolds that can accommodate recurrent dynamic loads and provide apposite culture substrates for cell attachment, proliferation, and differentiation [16–24]. In the past few decades, the physicochemical aspects of tissue culture substrates have been found to be critical in regulating cell function and fate. For example, anchorage-dependent cells, such as myoblasts, sense the mechanical stiffness of the underlying substrate and consequently modulate protein expression, morphology, and cytoskeleton organization [25]. In addition, cells exhibit a higher spreading area on the substrate with compliant mechanical stiffness than softer or stiffer substrates [26]. Moreover, skeletal muscle cells undergo contraction that depends on substrate stiffness [27], and display myosin/actin striation on mechanically compliant substrates compared to rigid ones. Engler and

Peer review under responsibility of KeAi Communications Co., Ltd.
* Corresponding author. Department of Chemical and Biological Engineering, University at Buffalo, The State University of New York, Buffalo, NY, 14260, USA.
** Corresponding author.
E-mail addresses: sandread@buffalo.edu (S.T. Andreadis), ccheng8@buffalo.edu (C. Cheng).

https://doi.org/10.1016/j.bioactmat.2020.12.022
Received 5 September 2020; Received in revised form 21 December 2020; Accepted 22 December 2020

co-workers demonstrated that the commitment of stem cells to a specific phenotype depends on matrix elasticity, with the preferential specification to brain tissues on soft substrates (0.1–1 kPa), muscle tissues on elastic platforms (8–17 kPa), and bone tissues on hard matrices (25–40 kPa) [28]. In general, mechanical signals emanating from culture substrates are key factors for controlling cell behavior and fate [29].

On the other hand, the adsorption of extracellular matrix proteins that modulate cell adhesion and subsequent cell response on tissue culture substrates is influenced by surface wettability [30]. Cantini and co-workers studied the myogenic differentiation of C2C12 on polystyrene substrates of different surface hydrophilicity adjusted by plasma treatment for different times [31]. Their study demonstrated that fibronectin adsorption and conformation depend on surface hydrophilicity, and in turn, affect cell density and differentiation. Accordingly, it is important to develop facile synthesis of biodegradable elastomers with mechanical and surface properties readily tuned for specific soft-tissue engineering applications.

A variety of chemical approaches have been adopted to prepare biodegradable elastomers with tunable properties for soft-tissue engineering. For instance, chemically crosslinked elastomers derived from poly(polyol sebacate) [32–34], poly(diol citrate) [35–37], poly(caprolactone fumarate) [38], and poly(trimethylene carbonate) [39] have been developed with a broad range of physicochemical properties. In addition, physically crosslinked aliphatic polyester scaffolds based on poly(lactic acid) (PLA) [40–43], poly(glycolic acid) (PGA) [44–46], poly (caprolactone) (PCL) [3,47,48], and poly(hydroxyalkanoate) (PHA) [49, 50] have been widely investigated in skeletal muscle regeneration. Recently, Zhao and co-workers developed dopamine/aniline hexamer-incorporated poly(citric acid-*co*-polycaprolactone) elastomers with tunable surface hydrophilicity achieved by varying the dopamine and aniline hexamer content. The synthesized elastomers supported attachment, proliferation, and myogenic differentiation of C2C12 cells [51]. Ma and co-workers reported electro-conductive PCL-based polyurethane elastomers that promoted the formation of nascent myotubes and myogenic differentiation [18]. Bo and co-workers illustrated that citrate-based biodegradable elastomer promoted *in vitro* myoblast proliferation, myotube formation and *in vivo* skeletal muscle regeneration [52]. Wanger and co-workers demonstrated the use of electrospun poly (ester urethane)urea biodegradable elastomer to micro-integrate skeletal muscle derived stem cells for the reconstruction of abdominal wall [19]. Although several types of biodegradable elastomers have shown promise for skeletal muscle tissue engineering, the curing step in elastomer formation often requires high temperatures (>100 °C) and/or long curing times (up to several days). Since photosensitive systems are employed in a variety of biofabrication technologies [53,54], the development of fast photocurable and biodegradable elastomers may be useful for skeletal muscle regeneration.

Recently, thiol-ene chemistry has been adopted for the preparation of polymeric biomaterials, including degradable elastomers [55–58]. As click reactions enabling robust and highly efficient synthesis, thiol-ene reactions can proceed via either free-radical addition or catalyzed Michael addition mechanism [59,60]. Free-radical thiol-ene reactions are particularly important, and can be induced by thermal- and photo-initiation [61,62]. Several types of thiol-ene elastomers with cleavable structures have been reported. Wooley and co-workers demonstrated the synthesis of isosorbid or quinic acid-based chemically crosslinked polymers, including elastomers, via thiol-ene crosslinking and post-curing at elevated temperature (≥100 °C) [63,64]. Robertson and co-workers reported thiol-ene elastomers derived from bio-based phenolic acids using a similar method [65]. Wang et al. investigated the preparation of chemically crosslinked degradable elastomer by thiol-ene reaction between cyclic acetal-based diallyl monomer and pentaerythritol tetrakis(3-mercaptopropionate) [66]. He and co-workers reported thermoplastic thiol-ene multiblock elastomers which were physically crosslinked through hydrogen-bonding [67]. Effective modulation of mechanical and structural properties of thiol-ene elastomers was demonstrated in some of these studies [63–65]. However, the application of thiol-ene elastomers for skeletal muscle tissue engineering has not been reported.

Therefore, there is a need to explore new strategies to develop fast photocurable biodegradable elastomers with well-tuned mechanical, structural, and physicochemical properties, and could support the formation of mature muscle fibers. In this work, we aim to address this need by synthesizing biodegradable elastomers with finely tuned mechanical properties and surface hydrophilicity via thiol-ene click reaction, thereby allowing fast photocuring and avoiding the application of elevated reaction conditions. Toward this aim, glycerol-based elastomers were synthesized and shown to support myogenic differentiation of skeletal muscle myoblasts toward multinucleated myotubes that were capable of spontaneous contractions.

2. Methods

2.1. Materials

4-Pentenoic anhydride (98%), 4-(dimethylamino)pyridine (DMAP, 99%), 4-penten-1-ol (99%), and trimethylpropane tris(3-mercaptopropionate) (TMPTMP) were purchased from Sigma-Aldrich. Glycerol (99+%) was purchased from Acros. Pyridine (99%) and dichloromethane (DCM) were purchased from Fischer Scientific, and DCM was dried by distillation over CaH_2 before use. 1,6-Hexanedithiol (HDT) was purchased from Alfa Aesar. 1,4-Butanediol bis(3-mercaptopropionate) (BDBMP) was purchased from TCI. Ethoxylated trimethylolpropane tri(3-mercaptopropionate) (ETTMP, $M_n = 700$) was obtained from Bruno Bock Chemische Fabrik GmbH & Co. KG. Chemicals and reagents were used as received unless otherwise stated.

2.2. Synthesis of GTP monomer

Glycerol (2.24 g, with 73.1 mmol OH, 1.0 equiv), 4-pentenoic anhydride (20.0 g, 110 mmol, 1.50 equiv), DMAP (1.34 g, 10.9 mmol, 0.15 equiv), and pyridine (8.68 g, 110 mmol, 1.50 equiv) were charged into a 100-mL round bottom flask, and the reaction mixture was stirred overnight before quenching with water for 3 h. The reaction mixture was diluted with DCM, and then washed with saturated $NaHSO_4$ aqueous solution (3 × 100 mL), 10 wt% $NaHCO_3$ aqueous solution (3 × 100 mL), and brine (2 × 100 mL). The organic layer was dried using anhydrous Na_2SO_4, concentrated to dryness, and then purified by flash chromatography using 1/9 (v/v) ethyl acetate/hexane as eluent to give the product as a colorless oil (7.57 g, 92% yield).

2.3. Synthesis of PP monomer

A 50-mL round bottom flask was charged with 4-penten-1-ol (2.59 g, 30.0 mmol, 1.0 equiv), 4-pentenoic anhydride (6.57 g, 36.0 mmol, 1.20 equiv), DMAP (0.55 g, 4.51 mmol, 0.15 equiv), and pyridine (2.85 g, 36.0 mmol, 1.2 equiv). The reaction mixture was allowed to proceed at room temperature (RT) for 24 h under stirring, and then quenched with water. The reaction mixture was diluted with DCM, and then washed with saturated $NaHSO_4$ aqueous solution (3 × 100 mL), 10 wt% $NaHCO_3$ aqueous solution (3 × 100 mL), and brine (2 × 100 mL). The organic layer was dried using anhydrous Na_2SO_4, concentrated to dryness to give the product as a colorless oil (4.50 g, 90% yield).

2.4. General preparation procedure for glycerol-based crosslinked elastomers

Glycerol-based elastomers were prepared using thiol-ene click chemistry to crosslink different combinations of thiol- and alkene-containing monomers upon irradiation with UV light in the presence of DMPA as photoinitiator. Two different elastomeric series were prepared: the first series included crosslinking of GTP with each of HDT,

BDBMP, TMPTMP, and ETTMP thiol monomers to obtain P(GTP-*co*-HDT), P(GTP-*co*-BDBMP), P(GTP-*co*-TMPTMP), and P(GTP-*co*-ETTMP) networks. In a typical experiment to prepare P(GTP-*co*-HDT), GTP (0.10 g, 0.29 mmol, 1.0 equiv of ene), HDT (6.66×10^{-2} g, 0.44 mmol, 1.0 equiv of thiol), and DMPA (1.62 mg, 1.0 wt %) were charged into a 10-mL vial (wrapped with aluminum foil to avoid undesirable photo-mediated polymerization), and then the reaction mixture was vortexed for 3 min before irradiation with UV light ($\lambda_{max} = 365$ nm; intensity $= 4 \times 10^5$ μJ/cm^2) for 5 min. Similarly, P(GTP-*co*-BDBMP), P(GTP-*co*-TMPTMP), and P(GTP-*co*-ETTMP) were prepared using reactants with equimolar ratio of thiol and alkene groups.

The second series included ternary elastomers prepared through thiol-ene copolymerization of GTP, PP, and BDBMP with varying $[ene]_{GTP}/[ene]_{GTP+PP}$ percentage (10%, 20%, 30%, 40%, 50%) in the feed. In brief, for the preparation of P(GTP-*co*-PP-*co*-BDBMP)-10%, BDBMP (0.10 g, 0.44 mmol, 1.0 equiv of thiol), PP (67 mg, 0.39 mmol, 0.90 equiv of ene), GTP (9.96 mg, 2.94×10^{-2} mmol, 0.10 equiv of ene), and DMPA (1.76 mg, 1.0 wt %) were placed in an aluminum foil-wrapped 10-mL vial. The reaction mixture was vortexed for 3 min, and then irradiated with UV light ($\lambda_{max} = 365$ nm; intensity $= 4 \times 10^5$ μJ/cm^2) for 5 min. Likewise, other tertiary elastomers were prepared.

2.5. Measurements

^{1}H NMR and ^{13}C NMR spectra of GTP and PP monomers were recorded using a Varian INOVA-500 spectrometer at RT, and the samples were dissolved in $CDCl_3$ containing 1.0 vol% tetramethylsilane (TMS) as an internal standard. FT-IR spectra of all elastomers were recorded using FT-IR spectrometer (Vertex 70, Bruker, MA) in the range of 4000–400 cm^{-1} with a resolution of 4 cm^{-1}. Raman spectra were recorded by a Renishaw inVia Raman system at an excitation wavelength of 514.5 nm.

Water contact angle of the elastomers was measured by the sessile drop method using a Ramé -Hart goniometer (Model 190, Ramé -Hart Instrument Co., Succasunna, NJ). In each measurement, a drop of deionized water (2 μL) was placed on the sample surface, and a real-time contact angle was obtained after 10 s using DROPimage software (Ramé -Hart Instrument Co.). The contact angle was taken as the average of five measurements.

The maximum swelling behavior of the elastomers was investigated in phosphate buffer solution (PBS, pH 7.4). After recording its dry weight (W_d), each sample was immersed in PBS and left to shake at 37 °C. After reaching equilibrium, inferred by constant weights, the samples were taken out from the PBS, wiped with filter paper to remove the surface solution, and then the final weight (w_s) was measured. The swelling ratios (%) were calculated as the average of three measurements.

In vitro enzymatic degradation of the glycerol-based elastomers was investigated using lipase enzyme from *Thermomyces lanuginosus* (≥100,000 U/g, Sigma). Elastomeric samples of circular shape (10 mm diameter × 1 mm thickness) were prepared, and their initial weights (w_1) were recorded. Each of the samples was incubated in 5 mL PBS (pH 7.4) solution of lipase (100 U/mL). Subsequently, the specimen was left to stir at 37 °C with a speed of 100 rpm; the lipase solution was replaced every 24 h to maintain the enzymatic activity. After specific time intervals, the sample was washed with distilled water, dried at 60 °C, and then the remaining weight (w_2) was recorded. The degradation percentage was calculated using the following equation:

$$\text{Mass remaining } (\%) = \frac{w_2}{w_1} \times 100\%$$

Protein adsorption on the elastomeric samples was evaluated using bovine serum albumin (BSA, VWR, Radnor, PA). Briefly, thin films of samples were prepared directly in a 48-well plate using 30 μL of reaction mixture per well, and then incubated overnight with PBS at 37 °C. After that, PBS was removed and BSA was added (250 μL, 1 mg/mL in PBS) to each well, followed by overnight incubation at 37 °C. The samples were washed with PBS to eliminate the non-adherent proteins and the amount of adsorbed protein on the surface was quantified using Commassie Blue assay kit (Thermo Fisher Scientific, Waltham, MA). The absorbance was measured at 595 nm using a Synergy4 plate reader (BioTek, Winooski, VT). Protein adsorption was reported as the average amount of BSA adsorption on three films of each sample.

The mechanical tests were performed using Instron tensile tester model 3343 with 50 N load cell instrument (Instron, Norwood, MA) and crosshead rate of 10 mm/min to obtain a stress-strain curve, Young's modulus, elongation at break, and tensile strength of all elastomers. The specimen for the mechanical test was prepared as follows: a dog-bone shaped mold of PLA was printed and fixed to a Petri dish in which SYLGARD 184 Silicone Elastomer (PDMS, 10/1 (w/w) base/curing agent) was cast. After baking at 40 °C for 24 h, PDMS was peeled off and served as a soft mold for the preparation of the specimens. Subsequently, 200 μL of the reaction mixture of each sample was added to the PDMS mold and crosslinked by UV irradiation for 5 min to obtain dog-bone shaped elastomer samples (total length: 24 mm; width of the ends: 4 mm: length of the narrow region: 12 mm: width of the narrow region: 2 mm) for the mechanical test. The elastomeric samples with almost smooth edges were separated from the PDMS mold by gentle bending of the of the PDMS layer. Three triplicates were measured for each sample. The maximum elongation and tensile strength were obtained from the stress (δ) – strain (ε) curves. Young's modulus was calculated from the slope of the elastic region on the stress-strain curves, whereas toughness was obtained from the area under the curves (toughness $= \int_{\varepsilon=0}^{\varepsilon=max} \sigma d\varepsilon$).

The glass transition temperature (T_g) of each elastomer was determined using differential scanning calorimetry (DSC; Q2000, TA Instruments, Waters LLC., New Castle, DE) at a heating rate 10 °C/min and a N_2 gas flow of 50 mL/min. The sample was heated from −90 °C to 100 °C, and the T_g value was taken from the second heating cycle as the midpoint of the heat capacity step change using the software of Universal Analysis (TA Instruments) [68].

The decomposition temperature (T_d) of each elastomer was determined by thermogravimetric analysis (TGA) using a TG 209 F1 instrument (NETZSCH Group, Germany). The sample was heated in the temperature range of 25 °C to 500 °C with a heating rate of 10 °C/min under an argon flow rate of 40 mL/min. T_d was taken at the first derivative peak of the thermogravimetric curve using the Proteus Thermal Analysis software [69].

Surface morphology of the binary glycerol-based elastomers was obtained using focused ion beam SEM (FIB-SEM, Zeiss Auriga, Germany) at an applied voltage of 20 kV. Prior to SEM imaging, all samples were sputtered with gold for 30 s at 30 mA to deposit a thin layer on the surface.

2.6. Cell culture

Human Myoblasts were purchased from Cookmyosite, Pittsburg, PA. Mouse myoblasts were isolated from the skeletal muscles of wild type mice from a C57BL/6 background according to the established protocol [70]. Human Myoblasts were cultured in high glucose Dulbecco's modified Eagle's medium (DMEM, Gibco, Grand Island, NY) supplemented with 20% fetal bovine serum (FBS, Atlanta Biologicals, Flowery Branch, GA), 50 μg/mL fetuin (Sigma-Aldrich), 0.5 mg/mL BSA, 10 ng/mL epidermal growth factor (EGF, produced in house), 1 ng/mL basic fibroblastic growth factor (bFGF, ORF Genetics, Iceland), 10 μg/mL insulin (Sigma-Aldrich), 0.4 μg/mL dexamethasone (Vedco Inc. Saint Joseph, MO), 10 μg/mL gentamycin (Gibco), 1% Antibiotic-Antimitotic (AA, Gibco), and 2.5 μg/mL plasmocin prophylactic (Invivogen, San Diego, CA). Mouse myoblasts were cultured in high glucose DMEM supplemented with 20% FBS, 10% horse serum (HS, Gibco), 0.5% chicken embryo extract (CEE, Accurate Chemical and

Scientific, Westbury, NY), 2.5 ng/mL bFGF, 10 μg/mL gentamycin, and 1% AA, and 2.5 μg/mL plasmocin prophylactic. The cells were seeded in Matrigel-treated T75 flasks at a cell density of 1000–3000 cells/cm^2 and incubated at 37 °C in a humidified atmosphere with 10% CO_2. Myoblasts were passaged prior to reaching 80% confluence using 0.25% Trypsin-EDTA (Gibco).

To initiate the myogenic differentiation of mononucleated myoblasts to multinucleated myotubes, after the cells reached above 80% confluence, the growth media was replaced with differentiation media composed of DMEM high glucose supplemented with 5% horse serum and 1% AA. The cells were cultured in differentiation media for 1 and 2 weeks, and the media was renewed every other day.

2.7. Cell viability and proliferation on elastomers

The elastomers with an estimated average thickness of ~90 μm were developed directly inside the 48-well plates, and washed by three cycles of ethanol (70%) and PBS solution, each for 30 min. The plates were further sterilized by UV light for 1 h prior to the experiments. All samples were treated with Matrigel (Corning®, Riverfront Plaza, NY) prior to cell seeding, through incubation with Matrigel (10% v/v in PBS) at 37 °C for 1 h [71,72]. Matrigel-treated polystyrene tissue culture plates (TCP) were used as controls in all experiments.

Cell viability assay and proliferation assay were performed to investigate the cytotoxicity of P(GTP-*co*-HDT), P(GTP-*co*-BDBMP), P(GTP-*co*-TMPTMP), and P(GTP-*co*-ETTMP) elastomers. Mouse myoblast cells were seeded at the density of 5000 cell/cm^2, and their viability was evaluated at day 1, 3, and 5 of culture using Live/Dead assay. At each time point, the cells were washed with PBS three times, and then incubated with Ethidium homodimer-1 (0.5 μM) and calcein AM (0.25 μM) (Thermo Fisher Scientific, Grand Island, NY) for 45 min. The fluorescent signals were observed using Zeiss Axio Observer Z1 (LSM 510; Zeiss, Oberkochen, Germany) equipped with a digital camera (ORCA-ER C4742-80; Hamamatsu, Bridgewater, NJ).

The proliferation of mouse and human myoblast cells was evaluated using Alamar Blue assay at day 1, 3, and 5 of seeding. Briefly, at each detection time, the culture medium was replaced with fresh media containing 10% (v/v) Alamar Blue. After 4 h incubation at 37 °C, 100 μL was transferred to 96-well black plates (Costar), and the fluorescence intensity was measured at 560/590 nm using Synergy4 fluorescence microplate reader. Alamar Blue at 10% (v/v) in medium served as blank.

2.8. Immunocytochemistry

Immunofluorescence against myosin heavy chain (MHC), sarcomeric α-actinin, and 4′,6-diamidino-2-phenylindole (DAPI) were performed at week one and two of differentiation in order to visualize the myogenic differentiation of human and mouse myoblasts. Briefly, the cells were first fixed at RT with 4% (w/v) paraformaldehyde for 10 min, followed by washing with PBS three times, and subsequently permeabilized with 0.1% (v/v) Triton X-100 in PBS for 10 min at RT. After three washes with PBS, the cells were blocked with blocking buffer (5 vol% goat serum in 0.01% (w/v) Triton X-100/PBS) at 25 °C for 1 h. After that, cells were incubated overnight with mouse-anti MHC (1:1000 dilution in blocking buffer, Millipore, Billerica, MA) and rabbit-anti actinin (1:200 dilution in blocking buffer, Abcam) monoclonal antibodies. After being washed with PBS three times, the samples were stained with Alexa Fluor 594 conjugated goat anti-mouse or 488 conjugated goat anti-rabbit antibodies (1:200 dilution in blocking buffer for 1 h, Thermo Fisher Scientific). The cells were counter-stained with DAPI as a nuclear marker for 1 min (1 μg/mL in PBS, Thermo Fisher Scientific). After being washed with PBS three times, the cells were observed using Zeiss Axio Observer Z1 (LSM 510; Zeiss, Oberkochen, Germany) equipped with a digital camera (ORCA-ER C4742-80; Hamamatsu, Bridgewater, NJ). The number, diameter, and length of myotubes, as well as the surface area covered by myotubes, were calculated using imageJ software.

2.9. RNA isolation cDNA synthesis and qRT-PCR

To verify myogenic differentiation of human myoblast cells on P(GTP-*co*-HDT), P(GTP-*co*-BDBMP), P(GTP-*co*-TMPTMP), and P(GTP-*co*-ETTMP) samples, the expression of the myogenic genes *MYF5, MYOD, MYOG, MRF4* with the housekeeping gene *RPL32* was investigated. Primers were obtained from the PrimerBank or the corresponding reference with the following 5'->3′ sequences;

MYF5; forward: AACCCTCAAGAGGTGTACCAC, reverse: AGGACTGTTACATTCGGGCAT.

MYOD; forward: CGCCATCCGCTATATCGAGG, reverse: CTGTAGTCCATCATGCCGTCG.

MYOG; forward: CAGTGCACTGGAGTTCAGCG, reverse: TTCATCTGGGAAGGCCACAGA [73].

MRF4; forward: CCCCTTCAGCTACAGACCCAA, reverse: CCCCCTGGAATGATCGGAAAC [73].

RPL32; forward: AGCGTAACTGGCGGAAAC; reverse: CGTTGTGGACCAGGAACTTC [74].

After two weeks of differentiation, cells were lysed and mRNA was isolated using RNeasy Mini Kit (QIAGEN, Valencia, CA) according to the manufacturer's extraction protocol, followed by measurement of the total concentration of mRNA using an ND 1000 Nanodrop (Life Technologies, USA). One μg mRNA was used to synthesize complementary deoxyribonucleic acid (cDNA) using a high-capacity cDNA reverse transcription kit (Thermo Fisher Scientific). qRT-PCR was conducted using Power SYBR® Green PCR MasterMix (Thermo Fisher Scientific) following the manufacturer's protocol, and carried out with an Applied Biosystems 7500 Fast Real-time PCR system with the following cycling conditions: 25 °C for 10 min, 37 °C for 60 min, and 95 °C for 5 min ΔC_T method was used to calculate the fold changes in gene expressions relative to the house keeping genes *RPL32*.

2.10. Spontaneous beating of myoblasts on elastomers

Zeiss Axio Observer Z1 (LSM 510; Zeiss, Oberkochen, Germany) equipped with a digital camera (ORCA-ER C4742-80; Hamamatsu, Bridgewater, NJ) was used to record the beating of mouse myotubes after 10 days of differentiation of myoblasts on P(GTP-*co*-HDT), P(GTP-*co*-BDBMP), P(GTP-*co*-TMPTMP), and P(GTP-*co*-ETTMP) elastomers. The spontaneous beating frequency was obtained by counting the number of beatings per minute. The density of beating myotubes on the surface was counted for 10 different fields of view (area = 0.55 mm^2 per field of view).

2.11. Statistical analysis

Statistical analysis was performed by One-Way ANOVA followed by the Fisher's least significant difference using Minitab software. The statistical significance between two mean values was analyzed using student *t*-test with respect to their standard deviations. The differences were considered significant at $P < 0.05$. Each experiment was repeated three times independently, with the data presented as mean ± standard deviation.

3. Results and discussion

3.1. Design, synthesis and structural characterization of thiol-ene elastomers

We employed thiol-ene click chemistry to prepare fast photocurable biodegradable elastomers with tunable mechanical and surface properties (Scheme 1). Di- and tri-thiols with a varying number of ester groups, chain length and hydrophilicity, including HDT, BDBMP, TMPTMP, and ETTMP (M_n = 700) were crosslinked with the glycerol-based GTP monomer upon UV irradiation. Moreover, we hypothesized copolymerizing BDBMP with a mixture of GTP and the ester-based PP

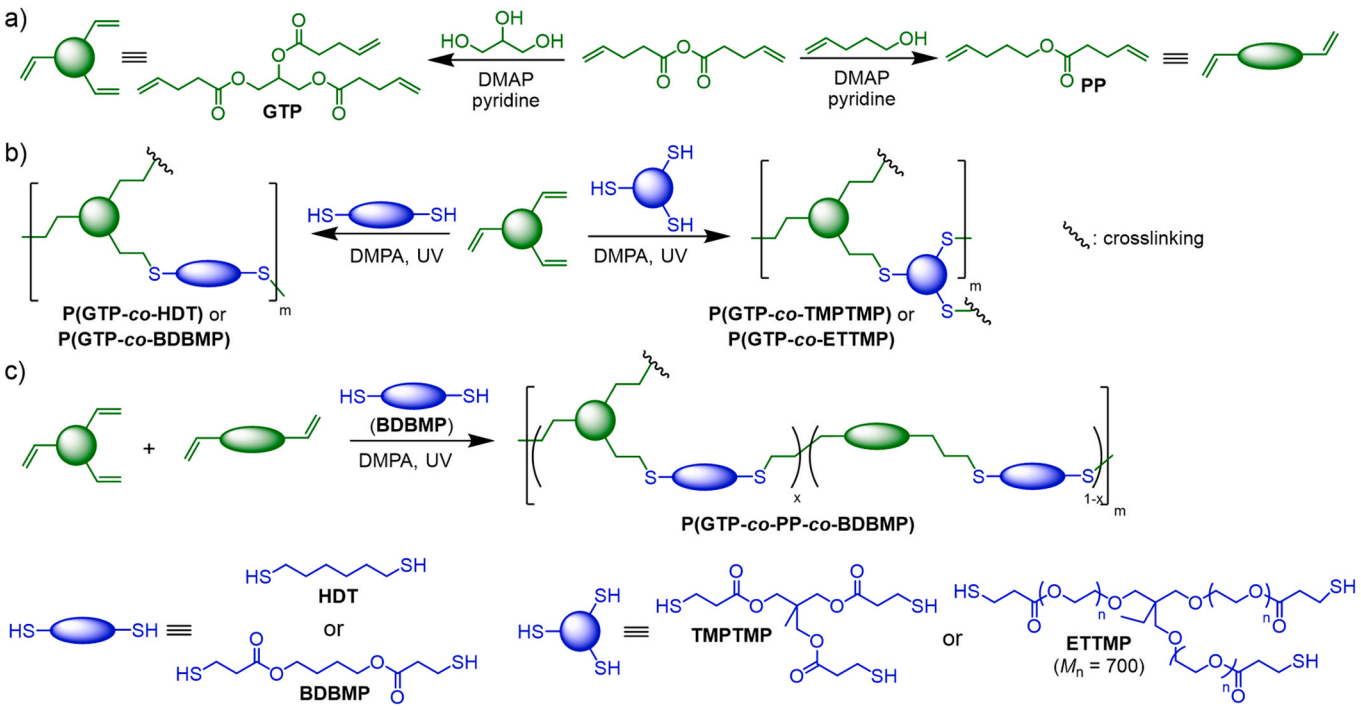

Scheme 1. Synthesis of a) GTP and PP alkene monomers, b) glycerol-based binary and c) ternary thiol-ene elastomers with tunable properties.

monomer might yield elastomers with a broad range of mechanical properties.

This thiol-ene synthetic approach has a number of attractive features. First, the utilization of UV-induced thiol-ene crosslinking strategy permits quick gelation by photocuring and avoids elevated temperatures and/or long curing times often required in thermally-induced curing process, and can enable the addition of bioactive agents without causing denaturation. Second, elastomers with copolymeric structures can be readily targeted by selecting thiol-ene monomers with flexible aliphatic structures, because they are not expected to possess significant crystallinity that would hinder their elastomeric properties [75]. Third, the synthesized ester-based alkene monomers and the commercially available thiol monomers provide a solid basis to tune the structures and properties of the resulting thiol-ene elastomers. The combination of bifunctional PP and trifunctional GTP as choices of alkene monomers can allow ready adjustment of mechanical properties of elastomers by simply changing their molar feed ratios to target different crosslinking density. The four thiol monomers, including both dithiols (HDT, BDBMP) and tri-thiols (TMPTMP and ETTMP), were chosen to further broaden the structure and property scopes of thiol-ene elastomers. Specifically, bifunctional BDBMP incorporating two ester bonds susceptible to biodegradation by proteases and lipases [76] may lead to relatively rapid degradation of elastomers. Moreover, among the tri-thiols that can form crosslinked thiol-based structural units of elastomers, TMPTMP can prompt crosslinking density and mechanical strength of elastomers, because it has a much less molecular weight than ETTMP. Furthermore, ETTMP and HDT can enhance hydrophilicity and hydrophobicity of the elastomers respectively, because the ethylene glycol units of ETTMP is hydrophilic and the alkyl chain of HDT is hydrophobic.

For the development of glycerol-based elastomers, GTP monomer was first synthesized by reacting the hydroxyl groups of glycerol with 4-pentenoic anhydride in the presence of pyridine, using DMAP as catalyst (Scheme 1a). The chemical structure of GTP monomer was confirmed by ^{1}H NMR, ^{13}C NMR, and ESI-MS analysis. Comparison of the ^{1}H NMR spectra of GTP (Fig. 1a) and glycerol (Fig. S1a) revealed the disappearance of the resonance signals of OH groups of glycerol at 4.37–4.47 ppm after functionalization, and the shift of –CH– and –CH_2- resonance signals from 3.37 to 3.30 ppm for glycerol to 4.28 and 4.13 ppm for GTP. The new signals for CH_2═CH- alkene protons appeared at 5.26–5.77 ppm. ^{13}C NMR data of GTP was in agreement with the chemical structure (Fig. S2a). ESI-MS analysis of GTP showed $[M+Na]^+$ m/z of 361.16 which matched exactly the theoretical value, providing additional evidence for the successful synthesis of GTP (Fig. S3a). For the development of elastomers with tunable mechanical properties, PP monomer with two reactive alkene groups was synthesized through the DMAP-catalyzed esterification reaction between 4-pentenoic anhydride and 4-pentenol in the presence of pyridine. It is worth to mention that PP monomer has chemical stability superior to 4-pentenoic anhydride which is susceptible to rapid cleavage by the components of cell culture media. The chemical structure of PP was verified by ^{1}H and ^{13}C NMR spectra (Fig. 1b, S2b) and ESI-MS analysis (Fig. S3b; found $[M+Na]^+$ m/z = 191.11, theoretical $[M+Na]^+$ m/z = 191.10).

GTP was crosslinked with a series of di- and tri-functional thiols (i.e., HDT, BDBMP, TMPTMP, ETTMP) to obtain P(GTP-*co*-HDT), P(GTP-*co*-BDBMP), P(GTP-*co*-TMPTMP), and P(GTP-*co*-ETTMP) of varying surface wettability, protein adsorption, degradability, and cell attachment behavior (Scheme 1b). In each experiment, GTP was mixed with an equimolar amount of thiol monomer, based on reactive groups, and subsequently irradiated with UV light (λ_{max} = 365 nm) in the presence of 2,2-dimethoxy-2-phenylacetophenone (DMPA) photoinitiator. In addition, thiol-ene crosslinking reactions with equimolar amounts of thiol group from BDBMP and ene group from GTP and PP, while varying $[ene]_{GTP}/[ene]_{GTP+PP}$ in the feed (Scheme 1c), resulted in P(GTP-*co*-PP-*co*-BDBMP)-10%, −20%, −30%, −40% and −50% networks of different mechanical characteristics (the percentage, 10–50%, corresponds to $[ene]_{GTP}/[ene]_{GTP+PP}$).

FT-IR and Raman spectroscopies were used to explore the extent of photopolymerization and network formation. FT-IR analysis of all binary and ternary copolymers showed quantitative disappearance of the stretching vibration of C–H of alkenes, S–H of thiol monomers, and C═C of alkenes at 3100, 2570, and 1650 cm^{-1}, respectively (Fig. 1c-d). Meanwhile, the stretching vibrations of S–H and C═C were markedly observed in FT-IR analysis of thiol and alkene monomers, respectively

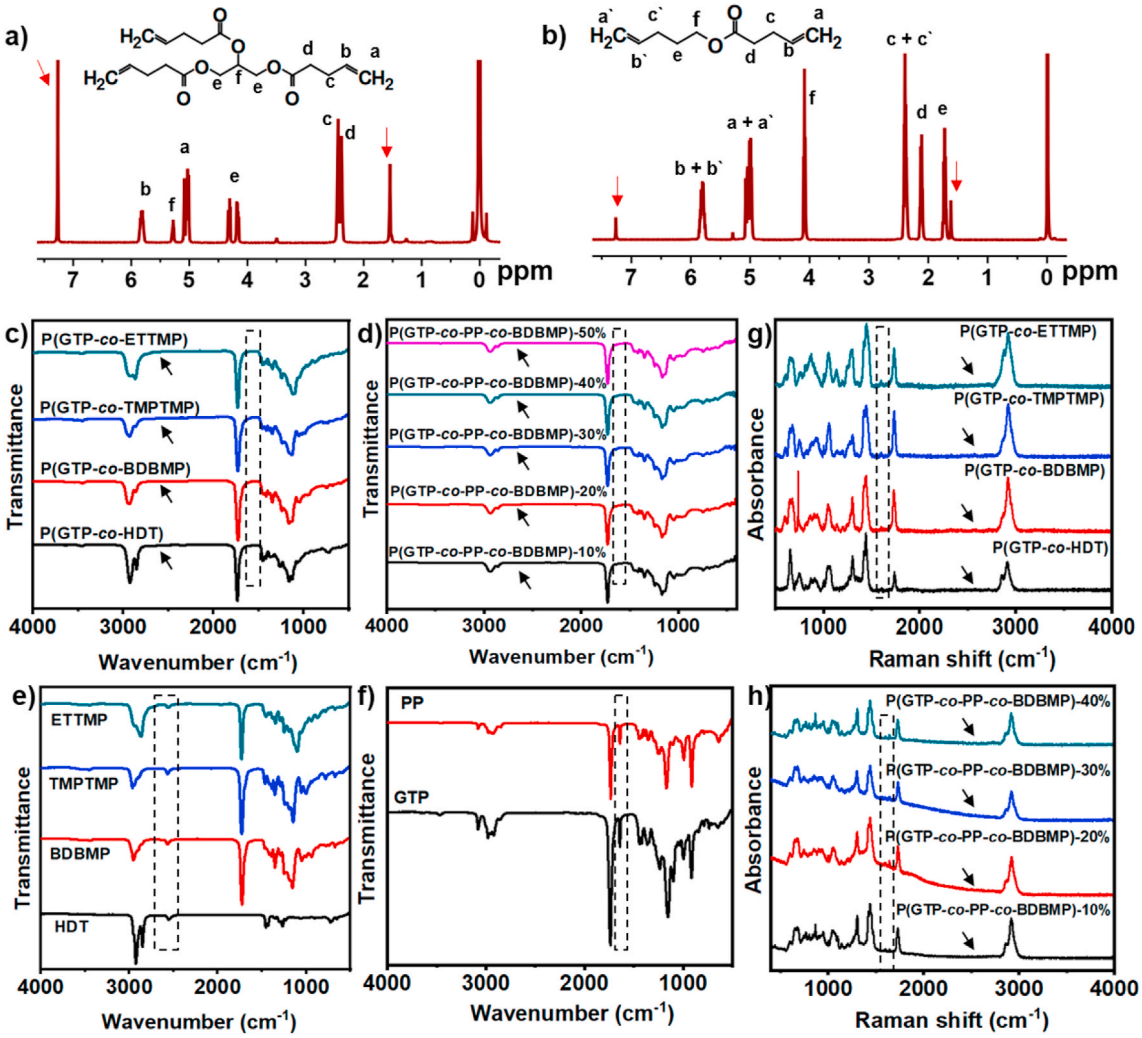

Fig. 1. ^{1}H NMR spectra of a) GTP and b) PP monomers in $CDCl_3$ (signals of solvent and water were marked by red arrows). FT-IR spectra of (c) glycerol-based binary elastomers, (d) P(GTP-*co*-PP-*co*-BDBMP) networks, (e) thiol crosslinkers, and (f) alkene monomers. Raman spectra of (g) glycerol-based binary elastomers and (h) P(GTP-*co*-PP-*co*-BDBMP) networks (black arrows indicate the disappearance of SH band). (For interpretation of the references to color in this figure legend, the reader is referred to the Web version of this article.)

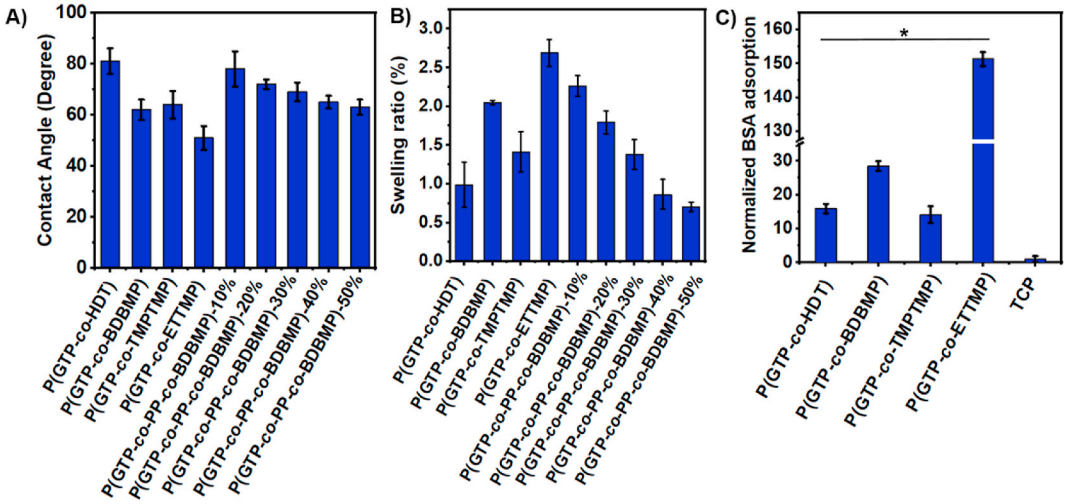

Fig. 2. (A) Water contact angle of the thiol-ene elastomers; (B) Swelling degree of glycerol-based elastomers and P(GTP-*co*-PP-*co*-BDBMP) networks; and (C) Protein adsorption on glycerol-based networks. (*P < 0.001).

(Fig. 1e-f). Complete consumptions of reactive SH and C═C upon thiol-ene crosslinking were corroborated by Raman analysis (Fig. 1g-h). Raman spectra of all networks confirmed the disappearance of the characteristic C═C and S–H bands at 1650 cm^{-1} and 2570 cm^{-1}, respectively. Taken together, the results demonstrated high reactivity of the thiol-ene reaction systems, enabling fast crosslinking upon UV irradiation.

3.2. Physicochemical properties of thiol-ene elastomers

Tuning the physicochemical properties of scaffolds' surface is critical in directing cell behavior [77]. Water contact angle between ~40° and ~80° has been demonstrated to promote cell attachment [78]. The thiol monomers were carefully chosen to develop elastomers with the appropriate range of surface wettability. Specifically, HDT was used to endow hydrophobicity to the networks due to its six-carbon aliphatic chain, while ETTMP was selected to develop elastomers with more hydrophilic surfaces owing to the hydrophilicity of poly(ethylene glycol) chains of ETTMP. Additionally, BDBMP and TMPTMP were introduced to develop surfaces with optimal hydrophilicity for cell attachment.

P(GTP-*co*-HDT), P(GTP-*co*-BDBMP), P(GTP-*co*-TMPTMP), and P(GTP-*co*-ETTMP) exhibited water contact angles of 81°, 62°, 64°, and 51°, respectively (Fig. 2A). Meanwhile, the water contact angles of P(GTP-*co*-PP-*co*-BDBMP) networks ranged between 63° and 78°. These results demonstrated facile modulation of the surface wettability of the elastomeric surfaces through judicious selection of the reacting monomers, and all networks displayed contact angles in the favorable range for cell attachment. The swellability data of glycerol-based binary elastomers revealed a swelling ratio between 0.99% (for P(GTP-*co*-HDT)) and 2.69% (for P(GTP-*co*-ETTMP) (Fig. 2B). For ternary P(GTP-*co*-PP-*co*-BDBMP) networks, the swelling ratio ranged from 0.70 to 2.26%, and decreased with increasing the GTP content due to the increase of the degree of crosslinking of the networks.

In vitro enzymatic degradation behavior of the elastomers was investigated by using lipase/PBS solution, which has been demonstrated to cleave ester bonds [18]. The degradation results showed that P(GTP-*co*-TMPTMP) and P(GTP-*co*-ETTMP) have the slowest degradation rate with 98.5 ± 0.11% and 98.1 ± 0.18% weight remaining respectively after 4 weeks (Fig. S7). This result is presumably attributed to the resistance of the highly crosslinked elastomers incorporating tri-thiols TMPTMP and ETTMP to degradation via surface erosion. During 4 weeks, P(GTP-*co*-BDBMP) exhibited higher degradation rate (89.6 ± 0.3% weight remaining) as compared with P(GTP-*co*-HDT) (96.7 ± 0.5% weight remaining). This result could be explained by the presence of two cleavable ester bonds in BDBMP, while the absence of cleavable ester bonds in HDT. For P(GTP-*co*-PP-*co*-BDBMP) elastomers, the degradation rate increased with the decrease of $[ene]_{GTP}/[ene]_{GTP+PP}$ mol% in the feed, with percentage of weight remaining between 89.4 ± 0.3% (for P(GTP-*co*-PP-*co*-BDBMP)-50%) and 84.4 ± 0.2% (P(GTP-*co*-PP--*co*-BDBMP)-10%). Overall, the results demonstrated the feasibility of tuning the degradation profile by the appropriate selection of ester-containing thiol-ene monomers.

Because tissue engineering substrates should be capable of immobilizing the extracellular matrix proteins secreted by cells to promote the formation of functional tissues, protein adsorption of P(GTP-*co*-HDT), P(GTP-*co*-BDBMP), P(GTP-*co*-TMPTMP), and P(GTP-*co*-ETTMP) was evaluated by using BSA as a model protein. The amount of BSA adsorbed was measured using Coomassie protein assay, and the results were normalized to BSA adsorption on polystyrene TCP. All elastomeric networks showed a significant increase in BSA adsorption relative to TCP. Indeed, relative to TCP, the P(GTP-*co*-HDT), P(GTP-*co*-BDBMP), P(GTP-*co*-TMPTMP), and P(GTP-*co*-ETTMP) elastomers exhibited 16.0 ± 1.4, 28.5 ± 1.4, 14.2 ± 2.5, and 151.3 ± 2.1 times increase in BSA adsorption (Fig. 2C). This observation was consistent with the higher swelling ratio of P(GTP-*co*-BDBMP) and P(GTP-*co*-ETTMP) elastomers relative to P(GTP-*co*-HDT) and P(GTP-*co*-TMPTMP) samples. The higher protein adsorption of P(GTP-*co*-ETTMP) relative to other samples was attributed to its significantly higher ($P < 0.05$) swelling ratio due to the innate hydrophilicity of the ethylene glycol units of ETTMP monomer (Fig. 2B). In a previous report, Vyner and co-workers suggested that the high surface water results in entropic gain during protein adsorption to the elastomers, leading to higher protein adsorption [79].

Mechanical properties of scaffolds have been shown to regulate cell behavior [80]. The stress-strain curves of glycerol-based binary and tertiary elastomers was obtained by using dog-bone shaped samples (Fig. S4). Their Young's modulus ranged from 0.07 ± 0.01 to 11.3 ± 0.8 MPa, and showed an increase with increasing GTP content (Table 1, Fig. S5). P(GTP-*co*-TMPTMP) and P(GTP-*co*-ETTMP) exhibited higher modulus of 11.3 ± 0.8 and 8.2 ± 0.3 MPa, respectively, relative to P(GTP-*co*-HDT) (6.1 ± 0.6 MPa) and P(GTP-*co*-BDBMP) (5.8 ± 0.4 MPa). This result indicates that tri-thiols (TMPTMP, ETTMP) resulted in higher degree of crosslinking and increased mechanical stiffness as compared to dithiols (HDT, BDBMP). The ultimate tensile strength of the networks ranged from 0.03 to 1.9 MPa, and the tensile strength of P(GTP-*co*-PP-*co*-BDBMP) networks increased with the GTP content owing to the formation of networks with a higher degree of crosslinking. The ultimate elongation of these networks was in the range of 15.2–445%, and the networks incorporating dithiols (HDT, BDBMP) displayed higher ultimate elongation than those incorporating tri-thiols (TMPTMP, ETTMP). For P(GTP-*co*-PP-*co*-BDBMP) networks, the percent elongation decreased with increasing the mole fraction of GTP. These results suggested that the mechanical properties could be tuned by the appropriate selection of crosslinking thiols or GTP/PP ratio. Of note, these thiol-ene elastomers generally have lower Young's modulus and ultimate tensile strength than poly(diol citrate) elastomers [36], presumably due to their differences in crosslinking density.

Thermal properties of all elastomeric samples, including T_g and T_d, were analyzed using DSC and TGA (Table 1, Fig. S6). The elastomers exhibited T_g values between −21.5 °C and −60.1 °C, suggesting network flexibility at RT. Noteworthily, P(GTP-*co*-TMPTMP) and P(GTP-*co*-ETTMP) networks displayed higher T_g values (−21.5 °C and −38.5 °C) than P(GTP-*co*-HDT) and P(GTP-*co*-BDBMP) (−51.1 °C and −44.4 °C). This result may be attributed to the restricted movement of segments of the networks containing TMPTMP and ETTMP tri-thiols relative to those incorporating HDT and BDBMP dithiols. Furthermore, P(GTP-*co*-PP-*co*-BDBMP) networks displayed similar T_g values, ranging from −65.1 to −58.9 °C. This result suggests that the average lengths of their segments for thermal motion were quite close, presumably because their crosslinking density was not particularly high. The T_d values of the networks were in the range of 369.4–382.4 °C. P(GTP-*co*-HDT) displayed the highest T_d value of 382.4 °C, presumably due to the lack of thermally unstable ester groups within HDT relative to other thiols. Additionally, all networks showed a major weight loss of over 90% in the first degradation phase, except for P(GTP-*co*-TMPTMP), which displayed a second degradation phase in the range of 400–480 °C (Fig. S6C-D). Its second degradation phase might be attributed to the formation of complex carbonaceous materials during thermal degradation of the crosslinks [66].

Overall, the broad physicochemical properties of the elastomers and the ease of designing tissue culture platforms with the desired properties are appealing for optimal differentiation of muscle progenitor cells. The elastomers in this study could be easily tailored to mimic the innate elasticity of muscle tissues, which has a significant impact on myogenic potential of myoblasts [81]. Previous reports showed that muscle tissues exhibit a broad range of mechanical properties, including Young's modulus of 51.27 ± 28.48 kPa for rat vastus lateralis muscle [82], 151.83 ± 50.30 kPa for pig medial muscle [82], and 11.2 MPa for activated skeletal muscle [83]. Our elastomers exhibit Young's modulus range between 70 kPa and 11.3 MPa, making them suitable for myogenic differentiation of various muscle progenitor cells. In addition, the high Young's modulus of the binary glycerol-based elastomers (5.8–11.3 MPa) put these elastomers in the upper range of Young's

Table 1
Mechanical and thermal properties of thiol-ene elastomers.

Sample	Young's modulus (MPa)	Elongation at break (%)	Tensile strength (MPa)	Toughness (kJ/m^3)	T_g (°C)	T_d (°C)
P(GTP-*co*-HDT)	6.1 ± 0.6	20.7 ± 1.9	1.0 ± 0.1	107.4 ± 21	−51.1	382.4
P(GTP-*co*-BDBMP)	5.8 ± 0.4	24.4 ± 1.7	1.2 ± 0.1	152.4 ± 36	−44.4	371.4
P(GTP-*co*-TMPTMP)	11.3 ± 0.8	18.8 ± 1.2	1.9 ± 0.1	177.4 ± 39	−21.5	376.8
P(GTP-*co*-ETTMP)	8.2 ± 0.3	15.2 ± 0.7	1.1 ± 0.1	86.4 ± 9.0	−38.5	378.1
P(GTP-*co*-PP-*co*-BDBMP)-10%	0.07 ± 0.01	445.4 ± 67.1	0.03 ± 0.01	79.4 ± 40.3	−64.8	369.4
P(GTP-*co*-PP-*co*-BDBMP)-20%	0.12 ± 0.01	208.2 ± 18.2	0.17 ± 0.02	191.1 ± 66.5	−65.1	370.7
P(GTP-*co*-PP-*co*-BDBMP)-30%	0.34 ± 0.01	114.6 ± 3.3	0.24 ± 0.01	140.1 ± 14.3	−64.7	374.1
P(GTP-*co*-PP-*co*-BDBMP)-40%	1.2 ± 0.1	75.0 ± 8.5	0.65 ± 0.04	247.4 ± 82.5	−63.2	376.8
P(GTP-*co*-PP-*co*-BDBMP)-50%	1.8 ± 0.1	58.7 ± 5.3	0.78 ± 0.06	233.0 ± 73.6	−58.9	376.1

modulus of skeletal muscle. The elastomers should be biodegradable and can provide a temporary support for the myoblasts until they regenerate the injured muscle tissues. Using HDT and BDBMP enabled changing the biodegradation profile of the binary glycerol-based elastomers without tremendous change of their stiffness; relative to P(GTP-*co*-HDT), P (GTP-*co*-BDBMP) degraded faster due to its high density of ester bonds. In a previous study of poly(diol citrate) elastomers, Yang et al. showed that the degradation rate of poly(diol citrate) followed the order: poly(1, 6-hexanediol-*co*-citrate) > poly(1,8-octanediol-*co*-citrate) > poly(1, 10-decanediol-*co*-citrate) > poly(1,12-dodecanediol-*co*-citrate) because of the density of hydrolysable ester bonds and the overall hydrophilicity of the copolymers decrease with this order [36]. The biodegradability of the ternary P(GTP-*co*-PP-*co*-BDBMP) elastomers was adjusted by varying the GTP content, which consequently changes crosslinking degree. These findings are corroborated by other studies that showed control of the biodegradation at the expense of the mechanical stiffness; less crosslinked elastomers degrade faster than more crosslinked elastomers [75,84].

3.3. Cell viability and proliferation on glycerol-based elastomers

Using polystyrene TCP as control, glycerol-based binary elastomers were chosen for further *in vitro* studies because of their structural simplicity. All substrates were treated with Matrigel using the same procedure and conditions prior to cell seeding. Matrigel is a complex mixture of extracellular matrix molecules derived from basement membrane matrix and has been widely used for cell culture [71,72]. The layer of Matrigel on a substrate is typically several hundred nanometers

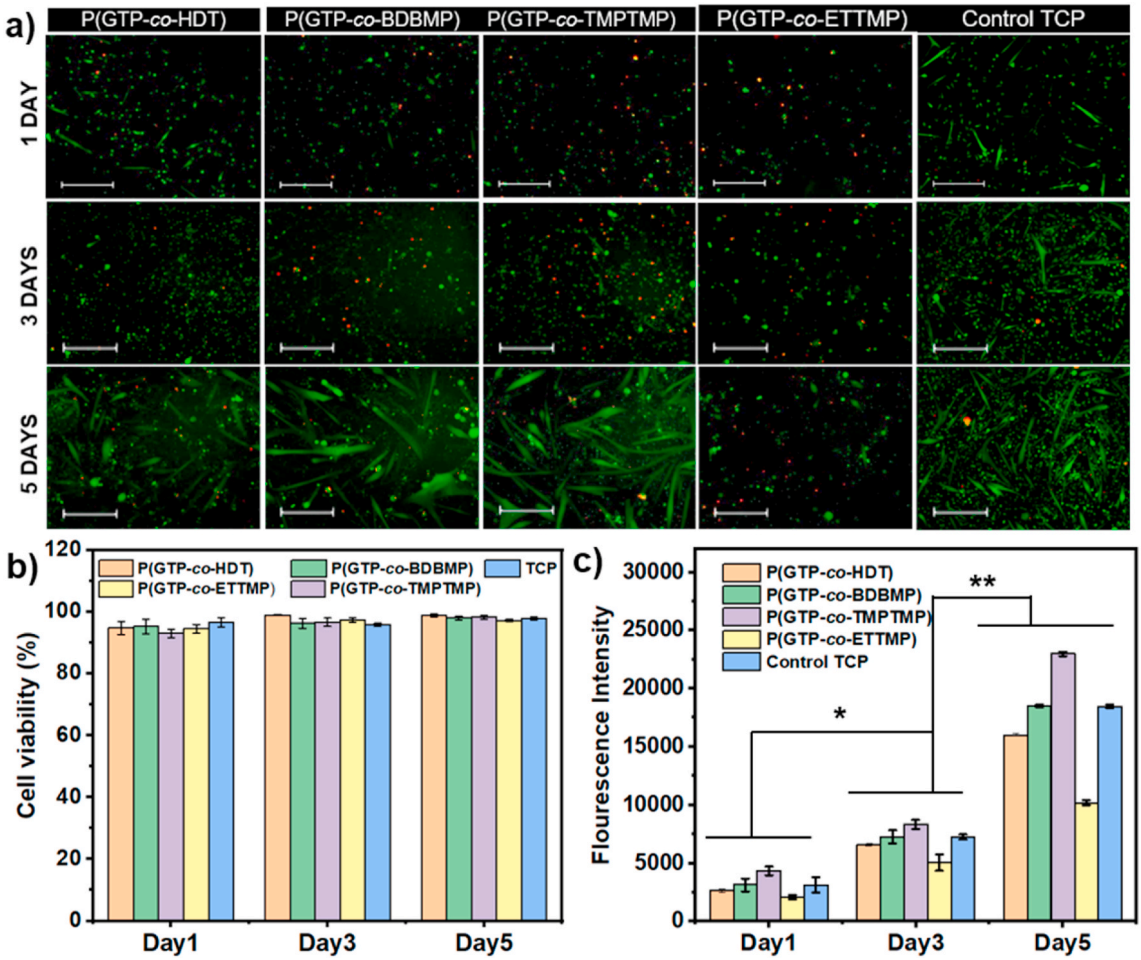

Fig. 3. (A) Live-dead of images of mouse myoblast on the elastomers on day 1, 3, and 5 of culture (scale bar 400 μm). (B) Quantification of live/dead assay images of mouse myoblast on the elastomers. (C) The proliferation of mouse myoblast on the glycerol-based elastomers analyzed by Alamar blue assay, $*p < 0.01$, $**p < 0.001$. (For interpretation of the references to color in this figure legend, the reader is referred to the Web version of this article.)

in thickness, which is much larger than the dimensions of biomolecules [85,86]. Because these thin layers are viscoelastic with elastic modulus of just a few hundred Pa [87], they do not block the interaction of cells with substrates, as evidenced by FT-IR microspectroscopic imaging data [88] and supported by the cell culture results on different substrates coated with Matrigel [86].

In vitro biocompatibility of P(GTP-*co*-HDT), P(GTP-*co*-BDBMP), P (GTP-*co*-TMPTMP), and P(GTP-*co*-ETTMP) elastomers was assessed using live/dead kit and Alamar blue assay. The viability and proliferation of mouse myoblast cells were examined after day 1, 3, and 5 of culture. Live/dead staining of cells showed that the myoblasts maintained their viability on the elastomers after 5 days of culture (green) and very few cells were dead (red) (Fig. 3a). Moreover, the cells displayed the normal spindle morphology similar to that on TCP, and remarkable myotubes were observed on P(GTP-*co*-HDT), P(GTP-*co*-BDBMP), P(GTP-*co*-TMPTMP), and TCP at day 5 post seeding as the cells reached above 80% confluence. Quantification of cell viability revealed more than 90% viable cells on the elastomers (Fig. 3b). These results demonstrated that all glycerol-based elastomers were biocompatible with no adverse effects on cell viability and proliferation.

The proliferation of mouse cells on the elastomers was measured and shown in Fig. 3c. After 3 days in culture, cells on P(GTP-*co*-TMPTMP) showed a significantly higher proliferation rate ($p < 0.05$) relative to those seeded on TCP, while myoblasts proliferated on P(GTP-*co*-BDBMP) displayed equivalent cell numbers ($p > 0.05$) as compared to those on TCP. Moreover, the number of cells was significantly reduced on P(GTP-*co*-HDT) and P(GTP-*co*-ETTMP) by 10% ($p < 0.05$) and 31% ($p < 0.05$) relative to the cell numbers on TCP, respectively. This result might be due to the decreased cell attachment on these elastomers, as a result of the relatively low stiffness of P(GTP-*co*-HDT) and the high surface hydrophilicity of P(GTP-*co*-ETTMP). There was 2.42 ($p < 0.01$), 2.55 ($p < 0.01$), 2.76 ($p < 0.01$), and 2.01($p < 0.01$)-times increase in number of growing cells at day 5 relative to day 1, on P(GTP-*co*-ETTMP), P(GTP-*co*-BDBMP), P(GTP-*co*-TMPTMP), and P(GTP-*co*-ETTMP) respectively, indicating that all these elastomers supported cell proliferation. Moreover, cells on P(GTP-*co*-BDBMP) and P(GTP-*co*-TMPTMP) (elastomers of intermediate hydrophilicity) showed significantly higher proliferation rates as compared to those seeded on more hydrophobic P(GTP-*co*-HDT) and more hydrophilic P(GTP-*co*-ETTMP), suggesting that tuning the surface properties of elastomers may be important for myoblast attachment and proliferation. Interestingly, despite the ability of the elastomers to adsorb considerable amounts of proteins, myoblast proliferation did not correlate with protein adsorption; P(GTP-*co*-ETTMP) showed the highest protein adsorption ability (see sec. 3.2) but led to the lowest proliferation rate among all substrates. This result may suggest that other material properties such as substrate stiffness and sureface wettability may be more important for cell attachment and proliferation, ultimately determining cell fate [53]. Of note, according to SEM imaging, all elastomers exhibited smooth morphology, indicating minimal contribution of surface roughness to cell attachment and proliferation (Fig. S8).

Similar to mouse myoblasts, human myoblasts also proliferated well on the elastomers (Fig. S9). After 5 days of culture, the numbers of cells on P(GTP-*co*-BDBMP) and P(GTP-*co*-TMPTMP) were 1.2 ($p < 0.05$) and 1.3 ($p < 0.01$)-fold higher relative to that on control TCP. On the other hand, the number of cells on P(GTP-*co*-ETTMP) was essentially equivalent to that on control TCP ($p > 0.05$), and P(GTP-*co*-HDT) resulted in slightly less cells than TCP. Overall, all elastomers supported the proliferation of mouse or human myoblasts and could potentially be promising substrates for growing myoblast cells for skeletal muscle regeneration.

3.4. Myogenic differentiation of human myoblast on glycerol-based elastomers

The development of *in vitro* models of skeletal muscles is critically important for pre-clinical drug testing, investigating disease mechanisms, identifying new therapeutic targets, and regenerating the injured muscle functions [89]. However, the prolonged culture of skeletal muscle is often restricted because of myotube delamination from the scaffolds after about one week of differentiation. Thus, it is desirable to support myoblast and myotube attachment for an adequate period of time to enable proper myoblast fusion, and consequently, the development of myotubes with higher maturation index [90]. Herein, the degree of human myoblast differentiation was assessed on the glycerol-based binary elastomers by immunostaining for myotube contractile machinery, MHC and sarcomeric α-actinin, at week 1 and 2 of differentiation. The results revealed the formation of an early network of multinucleated myotubes on the elastomers and TCP at week 1 of differentiation (Fig. S10a), with myotubes covering between 27.2 ± 4.2 to $62.0 \pm 4.0\%$ of the surface area (Fig. S10b). Interestingly, at week 2 of differentiation, the myotubes on elastomers continued their maturation, resulting in higher expression of MHC and sarcomeric α-actinin (Fig. S11); whereas significant detachment of myotubes was observed from TCP, resulting in significantly decreased coverage of the surface area as well as incomplete myotube maturation (Fig. S11).

The influence of the elastomers' physicochemical properties on human myoblast differentiation and myotube characteristics was assessed on week 2 of differentiation. Myotubes on the substrates were visualized by high magnification immunofluorescence images of MHC and sarcomeric α-actinin (Fig. 4A(a)). Moreover, immunofluorescence for MHC and sarcomeric α-actinin was employed to evaluate the surface area covered by myotubes. The myotube coverage area increased to $47.0 \pm 1.5\%$ and $64.3 \pm 1.8\%$, respectively, on P(GTP-*co*-BDBMP) and P (GTP-*co*-TMPTMP) elastomers at week 2 of differentiation; meanwhile, there was a severe decline in the area covered by myotubes on TCP (merely $0.90 \pm 0.01\%$; Fig. 4B). Quantification of myotube diameters revealed 2.7-, 2.1-, 3.3-, and 1.8-fold increase ($P < 0.05$) on P(GTP-*co*-HDT), P(GTP-*co*-BDBMP) and P(GTP-*co*-TMPTMP), and P(GTP-*co*-ETTMP), respectively, as compared to TCP (Fig. 4C).

Besides the myotube detachment, on TCP there was also an abundance of cells that were negative for MHC and sarcomeric α-actinin (Fig. 4A(a), right image). This result could be explained by the premature detachment of myotubes from TCP before reaching maturation, resulting in myotubes of thinner diameters. It is worth to mention that the unavoidable background fluorescence from the elastomers on DAPI channels interfered with the clear observation of the nuclei by immunostaining. Instead, this issue was resolved by H&E staining that revealed incorporation of a large number of nuclei (>50) in myotubes, especially on P(GTP-*co*-BDBMP) and P(GTP-*co*-TMPTMP), indicating superior myoblast fusion on the elastomers (Fig. 4A(b)). Immunostaining for the muscle-specific intermediate filament protein, desmin [91,92] on week two of differentiation provided further evidence for the ability of the elastomers to support long-term culture, revealing a higher percentage of area covered by desmin+ myotubes relative to TCP (Fig. 4A(c)). Overall, our results suggest that these elastomers prevent premature myotube detachment enabling long-term culture and maturation.

Myoblast differentiation on elastomers was evaluated by qRT-PCR for myogenic regulatory factors, *MYF5*, *MYOD*, myogenin (*MYOG*) and *MRF4* on day 10 of differentiation. As myoblasts progress through differentiation, they down-regulate the expression of the early and intermediate markers, *MYF5* and *MYOD;* and upregulate the expression of late differentiation markers *MYOG* and *MRF4* [93,94]. The results showed small but significant down-regulation of MYF5 expression on P (GTP-*co*-BDBMP) ($P < 0.05$), P(GTP-*co*-TMPTMP) ($P < 0.05$), and P (GTP-*co*-ETTMP) ($P < 0.05$) relative to TCP (Fig. 4D). There were no significant differences in the expression level of the intermediate marker, *MYOD,* between the cells cultured on elastomers and TCP. Notably, myoblasts cultured on the elastomers exhibited remarkable upregulation of *MYOG* and the late myogenic factor *MRF4,* as compared to cells on TCP ($P < 0.05$). It is worth noting that the disparities in the

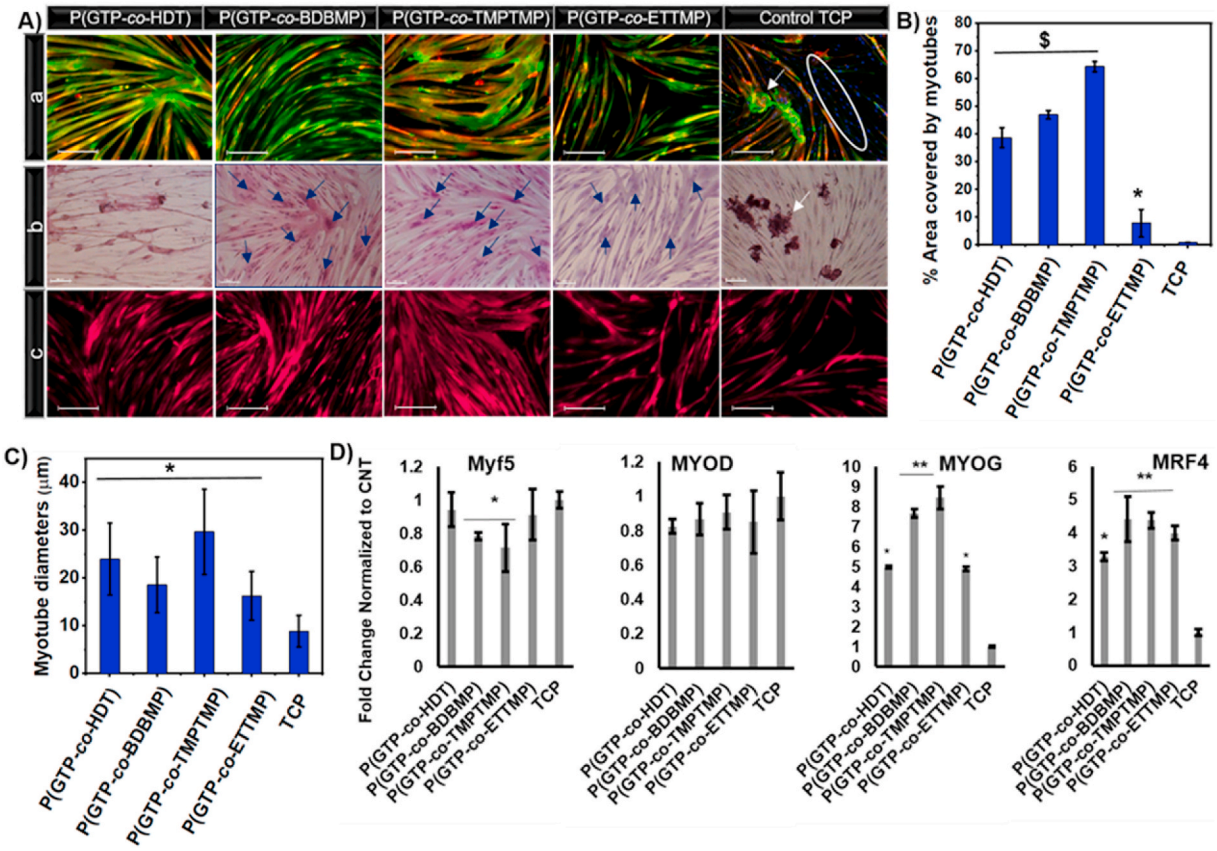

Fig. 4. (A) High magnification images of immunofluorescence staining for MHC and sarcomeric α-actinin (scale bar 200 μm) (a), H&E staining (scale bar 100 μm) (b), and immunostaining for desmin (scale bar 200 μm) (c), after two weeks of differentiation of human myoblasts on the indicated elastomers. (B and C) Quantification of myotube diameters and % area covered by myotubes after two weeks of differentiation on the indicated elastomers and TCP. (D) qRT-PCR of myogenic regulatory factors Myf5, MyoD, MyoG, and MRF4 after 10 days of differentiation on the indicated elastomers. The white circle represents MHC negative cells. White arrows show detached myotubes; blue arrows point to myotubes with more than 5 nuclei. (* denotes $P < 0.05$ as compared to TCP, $ denotes $P < 0.0001$ as compared to TCP, and ** denotes $P < 0.05$ as compared to all other samples.). (For interpretation of the references to color in this figure legend, the reader is referred to the Web version of this article.)

expression levels of the *MYOG* and *MRF4* between the elastomers (higher *MYOG* and *MRF4* expression on P(GTP-*co*-BDBMP) and P(GTP-*co*-TMPTMP) relative to P(GTP-*co*-HDT) and P(GTP-*co*-ETTMP)) are in line with higher myotube coverage area on these elastomers, indicating the critical importance of fine-tuning their properties for efficient myogenic differentiation. Overall, the qRT-PCR results suggested that the glycerol-based elastomers with tunable physicochemical characteristics enhance human myoblast differentiation as compared to TCP, thereby providing promising substrates for skeletal muscle regeneration.

3.5. Myogenic differentiation of mouse myoblasts on glycerol-based elastomers

To further investigate the influence of the elastomer characteristics on muscle contractility, we employed mouse myoblasts that have been shown to exhibit spontaneous beating associated with electrical activity resulting from an interplay of ionic currents (i.e., Na^+, Ca^{2+} and Ca^{2+}-activated K^+ currents) [95]. Immunofluorescence staining for myogenic-specific proteins, MHC and sarcomeric α-actinin was used to evaluate myotube formation. After one week of differentiation, myotubes on P(GTP-*co*-BDBMP) and P(GTP-*co*-TMPTMP) showed widespread interconnected MHC and sarcomeric α-actinin with highly organized structures (Fig. S12). However, cells on P(GTP-*co*-HDT) and P(GTP-*co*-ETTMP) exhibited random organization of sarcomeric α-actinin with the formation of scattered myotubes. Quantitative analysis of immunofluorescence images after one week of differentiation revealed higher surface coverage of myotubes on P(GTP-*co*-TMPTMP) (75.1 ± 4.4%) relative to TCP (38.7 ± 7.8%), while that on P(GTP-*co*-BDBMP) (39.9 ± 2.4%) was similar to that on TCP (Fig. 5B). Additionally, P(GTP-*co*-HDT) and P(GTP-*co*-ETTMP) exhibited significantly lower surface coverage of 18.7 ± 3.8% and 22.0 ± 17.1%, respectively, as compared to TCP.

After two weeks of differentiation, immunofluorescence staining revealed that myotubes on TCP were detached from the surface and their coverage area decreased to 11.8 ± 2.6% (Fig. 5A). On the other hand, the P(GTP-*co*-HDT), P(GTP-*co*-BDBMP), P(GTP-*co*-TMPTMP), and P(GTP-*co*-ETTMP) elastomers showed 1.6, 3.9, 4.6 and 4.1-fold increase in myotube coverage area relative to TCP ($p < 0.05$) (Fig. 5B). This result suggested that the elastomers support myotube attachment and stability on the surface. The higher myotube coverage area on P(GTP-*co*-BDBMP) and P(GTP-*co*-TMPTMP) elastomers relative to P(GTP-*co*-HDT) and P(GTP-*co*-ETTMP) after the first and second weeks of differentiation may reflect the importance of surface hydrophilicity in supporting mouse myoblast differentiation and myotube attachment. The discrepancy between the performance of P(GTP-*co*-HDT) in supporting myogenic differentiation of human but not mouse myoblasts (Figs. 4A and 5A) might be due to mouse myotube beating, which increased the likelihood of detachment from the surface.

Furthermore, these glycerol-based elastomers supported the development of muscle function as evidenced by mouse myotube beating, with contractions starting as soon as 5 days of treatment with differentiation media and continued for at least two weeks – the duration of the experiment. Interestingly, while beating and contraction accelerated

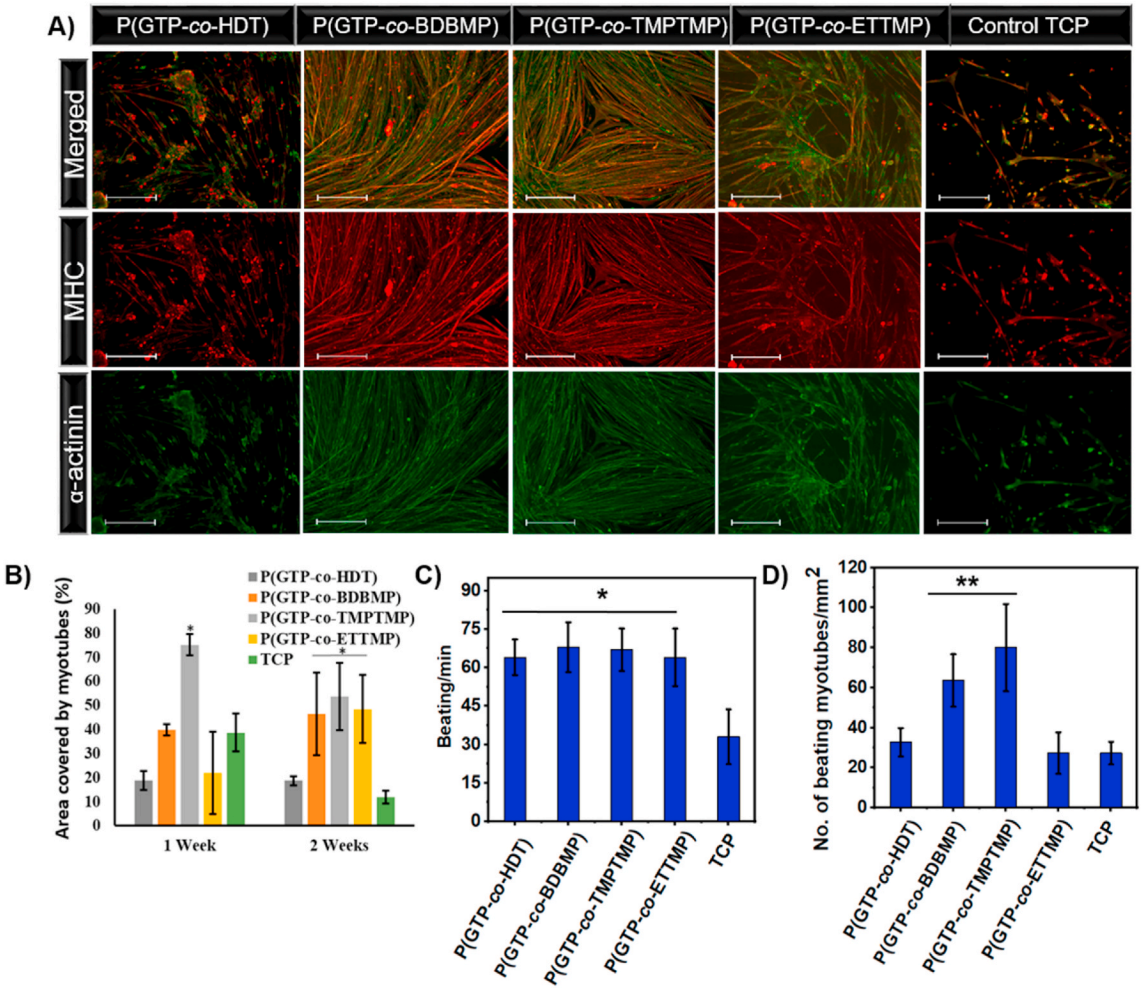

Fig. 5. (A) Immunostaining for MHC (red), sarcomeric α-actinin (green), and DAPI (blue) after two weeks of differentiation of mouse myoblasts on the indicated surfaces (scale bar 400 μm). (B) Quantification of myotube coverage area after one and two weeks of differentiation of mouse myoblasts. (C) The number of beating myotubes per mm^2, and (D) spontaneous beating frequency of mouse myotubes on glycerol-based elastomers after 10 days of differentiation. (*P < 0.005, and **P < 0.001). (For interpretation of the references to color in this figure legend, the reader is referred to the Web version of this article.)

the detachment of myotubes from the hard TCP substrate, the myotubes on the elastomers continued to beat and no significant detachment was observed. Measurements of spontaneous myotube beating revealed significantly higher myotube beating frequency on the elastomers as compared to TCP (TCP: 33 ± 10.7; P(GTP-*co*-HDT): 64 ± 6.9; P(GTP-*co*-BDBMP): 68 ± 9.7; P(GTP-*co*-TMPTMP): 66 ± 8.3; and P(GTP-*co*-ETTMP): 63 ± 11.1 beat/min, n = 5, p < 0.005 compared to TCP; Fig. 5C). Moreover, P(GTP-*co*-BDBMP), P(GTP-*co*-TMPTMP) exhibited higher density of beating myotubes (63.6 ± 13.1 and 80.0 ± 21.8 myotube/mm^2 respectively) as compared to the density of beating myotubes on TCP (27.3 ± 5.6 myotube/mm^2; n = 5, p < 0.001) (Fig. 5D). In agreement, immunostaining for MHC and sarcomeric α-actinin showed the formation of interconnected networks of multi-nucleated myotubes on P(GTP-*co*-BDBMP) and P(GTP-*co*-TMPTMP) relative to TCP. Overall, these results indicated that glycerol-based elastomers supported myotube surface adhesion and the development of contractile function.

4. Conclusion

Biocompatible elastomers with tunable surface hydrophilicity, degradability, and mechanical stiffness were developed using UV-induced thiol-ene click chemistry. GTP monomer was synthesized and then crosslinked with carefully selected thiol monomers, including HDT, BDBMP, TMPTMP, and ETTMP, via 5-min UV-irradiation at room temperature to quickly generate a series of binary elastomeric networks with a broad range of biophysical properties. Ternary elastomeric networks with tunable mechanical properties were also prepared through thiol-ene copolymerization of different ratios of GTP/PP with BDBMP. Young's moduli of the networks ranged from 0.07 MPa to 11.3 MPa, and higher mechanical strength was obtained from networks incorporating tri-thiols, rather than dithiols. Moreover, the networks displayed a wide range of ultimate elongation from 15.2 to 445%. Surface wettability measurements revealed their water contact angles in the range of 51.0–81.0°, while the hydrophilicity of the networks was significantly affected by the type of thiol monomer in the following order: P(GTP-*co*-ETTMP) > P(GTP-*co*-BDBMP) > P(GTP-*co*-TMPTMP) > P(GTP-*co*-HDT). All elastomers showed much higher adsorption of the model protein BSA than TCP. Biological assessment revealed that they all supported myoblast proliferation, while P(GTP-*co*-BDBMP) and P(GTP-*co*-TMPTMP) also enhanced myogenic differentiation of human and mouse myoblasts, to a greater extent as compared to TCP. Notably, in contrast to TCP, P(GTP-*co*-BDBMP) and P(GTP-*co*-TMPTMP) networks supported long-term adhesion and enhanced contractility of myotubes. Overall, these glycerol-based elastomers with tunable degradability, wettability and mechanical stiffness may provide a promising platform for engineering functional skeletal muscle for tissue regeneration and drug testing. Moreover, their remarkable photocurability can potentially

allow 3D-priniting of biodegradable elastomeric scaffolds, which may find broad applications in tissue engineering.

Declaration of competing interest

There is no conflict of interest to declare.

Acknowledgements

M. A. Mohamed acknowledges the Egyptian Ministry of Higher Education and Scientific Research for supporting him during his PhD study at the University at Buffalo.

Appendix A. Supplementary data

Supplementary data to this article can be found online at https://doi.org/10.1016/j.bioactmat.2020.12.022.

Author contributions

M. A. Mohamed conceived the project, and conducted the synthesis, characterization, and physicochemical properties study of the thiol-ene elastomers. J. Caserto contributed to the chemical characterization study. M. A. Mohamed and A. Shahini performed studies on cell viability, proliferation, and myogenic differentiation. N. Rajabian contributed to H & E staining. A. M. A. El-Sokkary, M. A. Akl, S. T. Andreadis, and C. Cheng supervised the project. M. A. Mohamed, A. Shahini, S. T. Andreadis, and C. Cheng contributed to the writing of the manuscript.

References

[1] F. Gattazzo, C. De Maria, A. Rimessi, S. Donà, P. Braghetta, P. Pinton, G. Vozzi, P. Bonaldo, Gelatin–genipin-based biomaterials for skeletal muscle tissue engineering, J. Biomed. Mater. Res. 106 (2018) 2763–2777, https://doi.org/10.1002/jbm.b.34057.

[2] B.J. Kwee, D.J. Mooney, Biomaterials for skeletal muscle tissue engineering, Curr. Opin. Biotechnol. 47 (2017) 16–22, https://doi.org/10.1016/j.copbio.2017.05.003.

[3] L. Wang, Y. Wu, B. Guo, P.X. Ma, Nanofiber yarn/hydrogel core–shell scaffolds mimicking native skeletal muscle tissue for guiding 3D myoblast alignment, elongation, and differentiation, ACS Nano 9 (2015) 9167–9179, https://doi.org/10.1021/acsnano.5b03644.

[4] A.D. Bach, J.P. Beier, J. Stern-Staeter, R.E. Horch, Skeletal muscle tissue engineering, J. Cell Mol. Med. 8 (2004) 413–422, https://doi.org/10.1111/j.1582-4934.2004.tb00466.x.

[5] S. Ostrovidov, S. Salehi, M. Costantini, K. Suthiwanich, M. Ebrahimi, R. B. Sadeghian, T. Fujie, X. Shi, S. Cannata, C. Gargioli, A. Tamayol, M.R. Dokmeci, G. Orive, W. Swieszkowski, A. Khademhosseini, 3D bioprinting in skeletal muscle tissue engineering, Small 15 (2019) 1805530, https://doi.org/10.1002/smll.201805530.

[6] R.L. Page, C. Malcuit, L. Vilner, I. Vojtic, S. Shaw, E. Hedblom, J. Hu, G.D. Pins, M. W. Rolle, T. Dominko, Restoration of skeletal muscle defects with adult human cells delivered on fibrin microthreads, Tissue Eng. 17 (2011) 2629–2640, https://doi.org/10.1089/ten.tea.2011.0024.

[7] S.A. Abbah, L.M. Delgado, A. Azeem, K. Fuller, N. Shologu, M. Keeney, M.J. Biggs, A. Pandit, D.I. Zeugolis, Harnessing hierarchical nano-and micro-fabrication technologies for musculoskeletal tissue engineering, Adv. Healthc. Mater. 4 (2015) 2488–2499, https://doi.org/10.1002/adhm.201500004.

[8] N. Narayanan, Z. Jia, K.H. Kim, L. Kuang, P. Lengemann, G. Shafer, V. Bernal-Crespo, Shihuan Kuang, M. Deng, Biomimetic glycosaminoglycan-based scaffolds improve skeletal muscle regeneration in a Murine volumetric muscle loss model, Bioact. Mater. 6 (2020) 1201–1213, https://doi.org/10.1016/j.bioactmat.2020.10.012.

[9] L. Zhou, J. Ge, M. Wang, M. Chen, W. Cheng, W. Ji, B. Lei, Injectable muscle-adhesive antioxidant conductive photothermal bioactive nanomatrix for efficiently promoting full-thickness skeletal muscle regeneration, Bioact. Mater. (2020) 1605–1607, https://doi.org/10.1016/j.bioactmat.2020.11.005.

[10] B. Amsden, Curable, biodegradable elastomers: emerging biomaterials for drug delivery and tissue engineering, Soft Matter 3 (2007) 1335–1348, https://doi.org/10.1039/B707472G.

[11] A.R. Webb, J. Yang, G.A. Ameer, Biodegradable polyester elastomers in tissue engineering, Expet Opin. Biol. Ther. 4 (2004) 801–812, https://doi.org/10.1517/14712598.4.6.801.

[12] C.J. Bettinger, Biodegradable elastomers for tissue engineering and cell–biomaterial interactions, Macromol. Biosci. 11 (2011) 467–482, https://doi.org/10.1002/mabi.201000397.

[13] Q. Chen, S. Liang, G.A. Thouas, Elastomeric biomaterials for tissue engineering, Prog. Polym. Sci. 38 (2013) 584–671, https://doi.org/10.1016/j.progpolymsci.2012.05.003.

[14] E. Bat, Z. Zhang, J. Feijen, D.W. Grijpma, A.A. Poot, Biodegradable elastomers for biomedical applications and regenerative medicine, Regen. Med. 9 (2014) 385–398, https://doi.org/10.2217/rme.14.4.

[15] W. Wu, R.A. Allen, Y. Wang, Fast-degrading elastomer enables rapid remodeling of a cell-free synthetic graft into a neoartery, Nat. Med. 18 (2012) 1148–1153, https://doi.org/10.1038/nm.2821.

[16] S.A. Young, S.E. Sherman, T.T. Cooper, C. Brown, F. Anjum, D.A. Hess, L.E. Flynn, B.G. Amsden, Mechanically resilient injectable scaffolds for intramuscular stem cell delivery and cytokine release, Biomaterials 159 (2018) 146–160, https://doi.org/10.1016/j.biomaterials.2018.01.008.

[17] R. van Lith, E.K. Gregory, J. Yang, M.R. Kibbe, G.A. Ameer, Engineering biodegradable polyester elastomers with antioxidant properties to attenuate oxidative stress in tissues, Biomaterials 35 (2014) 8113–8122, https://doi.org/10.1016/j.biomaterials.2014.06.004.

[18] Z. Deng, Y. Guo, X. Zhao, L. Li, R. Dong, B. Guo, P.X. Ma, Stretchable degradable and electroactive shape memory copolymers with tunable recovery temperature enhance myogenic differentiation, Acta Biomater. 46 (2016) 234–244, https://doi.org/10.1016/j.actbio.2016.09.019.

[19] K. Takanari, R. Hashizume, Y. Hong, N.J. Amoroso, T. Yoshizumi, B. Gharaibeh, O. Yoshida, K. Nonaka, H. Sato, J. Huard, W.R. Wagner, Skeletal muscle derived stem cells microintegrated into a biodegradable elastomer for reconstruction of the abdominal wall, Biomaterials 113 (2017) 31–41, https://doi.org/10.1016/j.biomaterials.2016.10.029.

[20] C. Xu, Y. Huang, L. Tang, Y. Hong, Low-initial-modulus biodegradable polyurethane elastomers for soft tissue regeneration, ACS Appl. Mater. Interfaces 9 (2017) 2169–2180, https://doi.org/10.1021/acsami.6b15009.

[21] C.K. Hagandora, J. Gao, Y. Wang, A.J. Almarza, Poly(glycerol sebacate): a novel scaffold material for temporomandibular joint disc engineering, Tissue Eng. 19 (2013) 729–737, https://doi.org/10.1089/ten.tea.2012.0304.

[22] A. Nieponice, L. Soletti, J. Guan, Y. Hong, B. Gharaibeh, T.M. Maul, J. Huard, W. R. Wagner, D.A. Vorp, In vivo assessment of a tissue-engineered vascular graft combining a biodegradable elastomeric scaffold and muscle-derived stem cells in a rat model, Tissue Eng. 16 (2010) 1215–1223, https://doi.org/10.1089/ten.tea.2009.0427.

[23] L. Wang, C. Wang, S. Wu, Y. Fan, X. Li, Influence of the mechanical properties of biomaterials on degradability, cell behaviors and signaling pathways: current progress and challenges, Biomater. Sci. 8 (2020) 2714–2733, https://doi.org/10.1039/D0BM00269K.

[24] J. Zhong, Y. Yang, L. Liao, C. Zhang, Matrix stiffness-regulated cellular functions under different dimensionalities, Biomater. Sci. 8 (2020) 2734–2755, https://doi.org/10.1039/C9BM01809C.

[25] A.J. Engler, M.A. Griffin, S. Sen, C.G. Bönnemann, H.L. Sweeney, D.E. Discher, Myotubes differentiate optimally on substrates with tissue-like stiffness: pathological implications for soft or stiff microenvironments, J. Cell Biol. 166 (2004) 877–887, https://doi.org/10.1083/jcb.200405004.

[26] C.M. Lo, H.B. Wang, M. Dembo, Y.L. Wang, Cell movement is guided by the rigidity of the substrate, Biophys. J. 79 (2000) 144–152, https://doi.org/10.1016/S0006-3495(00)76279-5.

[27] A. Engler, L. Bacakova, C. Newman, A. Hategan, M. Griffin, D. Discher, Substrate compliance versus ligand density in cell on gel responses, Biophys. J. 86 (2004) 617–628, https://doi.org/10.1016/S0006-3495(04)74140-5.

[28] A.J. Engler, S. Sen, H.L. Sweeney, D.E. Discher, Matrix elasticity directs stem cell lineage specification, Cell 126 (2006) 677–689, https://doi.org/10.1016/j.cell.2006.06.044.

[29] D.E. Discher, P. Janmey, Y.-l. Wang, Tissue cells feel and respond to the stiffness of their substrate, Science 310 (2005) 1139, https://doi.org/10.1126/science.1116995.

[30] G. Altankov, V. Thom, T. Groth, K. Jankova, G. Jonsson, M. Ulbricht, Modulating the biocompatibility of polymer surfaces with poly(ethylene glycol): effect of fibronectin, J. Biomed. Mater. Res. 52 (2000) 219–230, https://doi.org/10.1002/1097-4636(200010)52:1<219::AID-JBM28>3.0.CO;2-F.

[31] M. Cantini, M. Sousa, D. Moratal, J.F. Mano, M. Salmerón-Sánchez, Non-monotonic cell differentiation pattern on extreme wettability gradients, Biomater. Sci. 1 (2013) 202–212, https://doi.org/10.1039/C2BM00063F.

[32] R. Dong, X. Zhao, B. Guo, P.X. Ma, Biocompatible elastic conductive films significantly enhanced myogenic differentiation of myoblast for skeletal muscle regeneration, Biomacromolecules 18 (2017) 2808–2819, https://doi.org/10.1021/acs.biomac.7b00749.

[33] D. Motlagh, J. Yang, K.Y. Lui, A.R. Webb, G.A. Ameer, Hemocompatibility evaluation of poly(glycerol-sebacate) in vitro for vascular tissue engineering, Biomaterials 27 (2006) 4315–4324, https://doi.org/10.1016/j.biomaterials.2006.04.010.

[34] Y. Wang, G.A. Ameer, B.J. Sheppard, R. Langer, A tough biodegradable elastomer, Nat. Biotechnol. 20 (2002) 602–606, https://doi.org/10.1038/nbt0602-602.

[35] A.K. Sharma, P.V. Hota, D.J. Matoka, N.J. Fuller, D. Jandali, H. Thaker, G. A. Ameer, E.Y. Cheng, Urinary bladder smooth muscle regeneration utilizing bone marrow derived mesenchymal stem cell seeded elastomeric poly(1,8-octanediol-*co*-citrate) based thin films, Biomaterials 31 (2010) 6207–6217, https://doi.org/10.1016/j.biomaterials.2010.04.054.

[36] J. Yang, A.R. Webb, S.J. Pickerill, G. Hageman, G.A. Ameer, Synthesis and evaluation of poly(diol citrate) biodegradable elastomers, Biomaterials 27 (2006) 1889–1898, https://doi.org/10.1016/j.biomaterials.2005.05.106.
[37] D. Gyawali, J.P. Kim, J. Yang, Bioactive materials 3, Highly photostable nanogels for fluorescence-based theranostics, Bioact. Mater. 3 (2018) 39–47, https://doi.org/10.1016/j.bioactmat.2017.03.001.
[38] E. Jabbari, S. Wang, L. Lu, J.A. Gruetzmacher, S. Ameenuddin, T.E. Hefferan, B. L. Currier, A.J. Windebank, M.J. Yaszemski, Synthesis, material properties, and biocompatibility of a novel self-cross-linkable poly(caprolactone fumarate) as an injectable tissue engineering scaffold, Biomacromolecules 6 (2005) 2503–2511, https://doi.org/10.1021/bm050206y.
[39] L.-Q. Yang, B. He, S. Meng, J.-Z. Zhang, M. Li, J. Guo, Y.-M. Guan, J.-X. Li, Z.-W. Gu, Biodegradable cross-linked poly(trimethylene carbonate) networks for implant applications: synthesis and properties, Polymer 54 (2013) 2668–2675, https://doi.org/10.1016/j.polymer.2013.03.059.
[40] J. Feng, X. Yan, K. Lin, S. Wang, J. Luo, Y. Wu, Characterization of poly(lactic acid) melt spun fiber aligned scaffolds prepared with hot pressing method, Mater. Lett. 214 (2018) 178–181, https://doi.org/10.1016/j.matlet.2017.12.005.
[41] K.D. McKeon-Fischer, J.W. Freeman, Characterization of electrospun poly(L-lactide) and gold nanoparticle composite scaffolds for skeletal muscle tissue engineering, J. Tissue Eng. Regen. Med. 5 (2011) 560–568, https://doi.org/10.1002/term.348.
[42] H. Tian, S. Bharadwaj, Y. Liu, H. Ma, P.X. Ma, A. Atala, Y. Zhang, Myogenic differentiation of human bone marrow mesenchymal stem cells on a 3D nano fibrous scaffold for bladder tissue engineering, Biomaterials 31 (2010) 870–877, https://doi.org/10.1016/j.biomaterials.2009.10.001.
[43] M. Xie, L. Wang, B. Guo, Z. Wang, Y.E. Chen, P.X. Ma, Ductile electroactive biodegradable hyperbranched polylactide copolymers enhancing myoblast differentiation, Biomaterials 71 (2015) 158–167, https://doi.org/10.1016/j.biomaterials.2015.08.042.
[44] Y. Ji, G.P. Xu, J.L. Yan, S.H. Pan, Transplanted bone morphogenetic protein/poly (lactic-*co*-glycolic acid) delayed-release microcysts combined with rat micromorselized bone and collagen for bone tissue engineering, J. Int. Med. Res. 37 (2009) 1075–1087, https://doi.org/10.1177/147323000903700412.
[45] S. Salehi, S. Ostrovidov, M. Ebrahimi, R.B. Sadeghian, X. Liang, K. Nakajima, H. Bae, T. Fujie, A. Khademhosseini, Development of flexible cell-loaded ultrathin ribbons for minimally invasive delivery of skeletal muscle cells, ACS Biomater. Sci. Eng. 3 (2017) 579–589, https://doi.org/10.1021/acsbiomaterials.6b00696.
[46] J. Xu, Y. Xie, H. Zhang, Z. Ye, W. Zhang, Fabrication of PLGA/MWNTs composite electrospun fibrous scaffolds for improved myogenic differentiation of C2C12 cells, Colloids Surf., B 123 (2014) 907–915, https://doi.org/10.1016/j.colsurfb.2014.10.041.
[47] M. Kim, W. Kim, G. Kim, Topologically micropatterned collagen and poly (ε-caprolactone) struts fabricated using the poly(vinyl alcohol) fibrillation/leaching process to develop efficiently engineered skeletal muscle tissue, ACS Appl. Mater. Interfaces 9 (2017) 43459–43469, https://doi.org/10.1021/acsami.7b14192.
[48] M. Yeo, H. Lee, G.H. Kim, Combining a micro/nano-hierarchical scaffold with cell-printing of myoblasts induces cell alignment and differentiation favorable to skeletal muscle tissue regeneration, Biofabrication 8 (2016) 35021/1–35021/12, https://doi.org/10.1088/1758-5090/8/3/035021.
[49] Y.-W. Wang, F. Yang, Q. Wu, Y.-c. Cheng, P.H.F. Yu, J. Chen, G.-Q. Chen, Effect of composition of poly(3-hydroxybutyrate-co-3-hydroxyhexanoate) on growth of fibroblast and osteoblast, Biomaterials 26 (2005) 755–761, https://doi.org/10.1016/j.biomaterials.2004.03.023.
[50] Y.-W. Wang, Q. Wu, G.-Q. Chen, Reduced mouse fibroblast cell growth by increased hydrophilicity of microbial polyhydroxyalkanoates via hyaluronan coating, Biomaterials 24 (2003) 4621–4629, https://doi.org/10.1016/S0142-9612(03)00356-9.
[51] X. Zhao, R. Dong, B. Guo, P.X. Ma, Dopamine-incorporated dual bioactive electroactive shape memory polyurethane elastomers with physiological shape recovery temperature, high stretchability, and enhanced C2C12 myogenic differentiation, ACS Appl. Mater. Interfaces 9 (2017) 29595–29611, https://doi.org/10.1021/acsami.7b10583.
[52] Y. Guo, M. Wang, J. Ge, W. Niu, M. Chen, W. Cheng, B. Lei, Bioactive biodegradable polycitrate nanoclusters enhances the myoblast differentiation and in vivo skeletal muscle regeneration via p38 MAPK signaling pathway, Bioact. Mater. 5 (2020) 486–495, https://doi.org/10.1016/j.bioactmat.2020.04.004.
[53] M.A. Mohamed, A. Fallahi, A.M.A. El-Sokkary, S. Salehi, M.A. Akl, A. Jafari, A. Tamayol, H. Fenniri, A. Khademhosseini, S.T. Andreadis, C. Cheng, Stimuli-responsive hydrogels for manipulation of cell microenvironment: from chemistry to biofabrication technology, Prog. Polym. Sci. 98 (2019) 101147, https://doi.org/10.1016/j.progpolymsci.2019.101147.
[54] H. Quan, T. Zhang, H. Xu, S. Luo, J. Nie, X. Zhu, Photo-curing 3D printing technique and its challenges, Bioact. Mater. 5 (2020) 110–115, https://doi.org/10.1016/j.bioactmat.2019.12.003.
[55] C.E. Hoyle, C.N. Bowman, Thiol–ene click chemistry, Angew. Chem. Int. Ed. 49 (2010) 1540–1573, https://doi.org/10.1002/anie.200903924.
[56] A.B. Lowe, Thiol-ene "click" reactions and recent applications in polymer and materials synthesis, Polym. Chem. 1 (2010) 17–36, https://doi.org/10.1039/B9PY00216B.
[57] M.J. Kade, D.J. Burke, C.J. Hawker, The power of thiol-ene chemistry, J. Polym. Sci. Polym. Chem. 48 (2010) 743–750, https://doi.org/10.1002/pola.23824.
[58] J. Zou, C.C. Hew, E. Themistou, Y. Li, C.K. Chen, P. Alexandridis, C. Cheng, Clicking well-defined biodegradable nanoparticles and nanocapsules by UV-induced thiol-ene cross-linking in transparent miniemulsions, Adv. Mater. 23 (2011) 4274–4277, https://doi.org/10.1002/adma.201101646.
[59] C.E. Hoyle, T.Y. Lee, T. Roper, Thiol–enes: chemistry of the past with promise for the future, J. Polym. Sci. Polym. Chem. 42 (2004) 5301–5338, https://doi.org/10.1002/pola.20366.
[60] D.P. Nair, M. Podgorski, S. Chatani, T. Gong, W. Xi, C.R. Fenoli, C.N. Bowman, The thiol-Michael addition click reaction: a powerful and widely used tool in materials chemistry, Chem. Mater. 26 (2014) 724–744, https://doi.org/10.1021/cm402180t.
[61] N.B. Cramer, S.K. Reddy, A.K. O'Brien, C.N. Bowman, Thiol−ene photopolymerization mechanism and rate limiting step changes for various vinyl functional group chemistries, Macromolecules 36 (2003) 7964–7969, https://doi.org/10.1021/ma034667s.
[62] L.M. Campos, K.L. Killops, R. Sakai, J.M. Paulusse, D. Damiron, E. Drockenmuller, B.W. Messmore, C.J. Hawker, Development of thermal and photochemical strategies for thiol−ene click polymer functionalization, Macromolecules 41 (2008) 7063–7070, https://doi.org/10.1021/ma801630n.
[63] T.S. Kristufek, S.L. Kristufek, L.A. Link, A.C. Weems, S. Khan, S.-M. Lim, A. T. Lonnecker, J.E. Raymond, D.J. Maitland, K.L. Wooley, Rapidly-cured isosorbide-based cross-linked polycarbonate elastomers, Polym. Chem. 7 (2016) 2639–2644, https://doi.org/10.1039/C5PY01659B.
[64] L.A. Link, A.T. Lonnecker, K. Hearon, C.A. Maher, J.E. Raymond, K.L. Wooley, Photo-cross-linked poly (thioether-*co*-carbonate) networks derived from the natural product quinic acid, ACS Appl. Mater. Interfaces 6 (2014) 17370–17375, https://doi.org/10.1021/am506087e.
[65] G. Yang, S.L. Kristufek, L.A. Link, K.L. Wooley, M.L. Robertson, Thiol–ene elastomers derived from biobased phenolic acids with varying functionality, Macromolecules 49 (2016) 7737–7748, https://doi.org/10.1021/acs.macromol.6b01018.
[66] K. Wang, J. Lu, R. Yin, L. Chen, S. Du, Y. Jiang, Q. Yu, Preparation and properties of cyclic acetal based biodegradable gel by thiol-ene photopolymerization, Mater. Sci. Eng. C 33 (2013) 1261–1266, https://doi.org/10.1016/j.msec.2012.12.024.
[67] H. Li, S. Thanneeru, L. Jin, C.J. Guild, J. He, Multiblock thermoplastic elastomers via one-pot thiol–ene reaction, Polym. Chem. 7 (2016) 4824–4832, https://doi.org/10.1039/C6PY00822D.
[68] H. Lin, E.V. Wagner, J.S. Swinnea, B.D. Freeman, S.J. Pas, A.J. Hill, S. Kalakkunnath, D.S. Kalika, Transport and structural characteristics of crosslinked poly(ethylene oxide) rubbers, J. Membr. Sci. 276 (2006) 145–161, https://doi.org/10.1016/j.memsci.2005.09.040.
[69] L. Li, P. Zhang, J. Liang, S.M. Guo, Phase transformation and morphological evolution of electrospun zirconia nanofibers during thermal annealing, Ceram. Int. 36 (2010) 589–594, https://doi.org/10.1016/j.ceramint.2009.09.030.
[70] A. Shahini, K. Vydiam, D. Choudhury, N. Rajabian, T. Nguyen, P. Lei, S. T. Andreadis, Efficient and high yield isolation of myoblasts from skeletal muscle, Stem Cell Res. 30 (2018) 122–129, https://doi.org/10.1016/j.scr.2018.05.017.
[71] C.S. Hughes, L.M. Postovit, G.A. Lajoie, Matrigel: a complex protein mixture required for optimal growth of cell culture, Proteomics 10 (2010) 1886–1890, https://doi.org/10.1002/pmic.200900758.
[72] H.K. Kleinman, G.R. Martin, Matrigel: basement membrane matrix with biological activity, Semin. Canc. Biol. 15 (2005) 378–386, https://doi.org/10.1016/j.semcancer.2005.05.004.
[73] B.R. McKay, C.E. O'Reilly, S.M. Phillips, M.A. Tarnopolsky, G. Parise, Co-expression of IGF-1 family members with myogenic regulatory factors following acute damaging muscle-lengthening contractions in humans, J. Physiol. 586 (2008) 5549–5560, https://doi.org/10.1113/jphysiol.2008.160176.
[74] A. Shahini, P. Mistriotis, M. Asmani, R. Zhao, S.T. Andreadis, NANOG restores contractility of mesenchymal stem cell-based senescent microtissues, Tissue Eng. 23 (2017) 535–545, https://doi.org/10.1089/ten.tea.2016.0494.
[75] X. Ding, Y. Chen, C.A. Chao, Y.-L. Wu, Y. Wang, Control the mechanical properties and degradation of poly(glycerol sebacate) by substitution of the hydroxyl groups with palmitates, Macromol. Biosci. 20 (2020) 2000101, https://doi.org/10.1002/mabi.202000101.
[76] Z. Wei, W. Wang, C. Zhou, C. Jin, X. Leng, Y. Li, X. Zhang, S. Chen, B. Zhang, K. Yang, In vitro degradation and biocompatibility evaluation of fully biobased thermoplastic elastomers consisting of poly(β-myrcene) and poly(l-lactide) as stent coating, Polym. Degrad. Stabil. 179 (2020) 109254, https://doi.org/10.1016/j.polymdegradstab.2020.109254.
[77] L. Ghasemi-Mobarakeh, M.P. Prabhakaran, M. Morshed, M.-H. Nasr-Esfahani, S. Ramakrishna, Electrospun poly(ε-caprolactone)/gelatin nanofibrous scaffolds for nerve tissue engineering, Biomaterials 29 (2008) 4532–4539, https://doi.org/10.1016/j.biomaterials.2008.08.007.
[78] T.J. Rivers, T.W. Hudson, C.E. Schmidt, Synthesis of a novel, biodegradable electrically conducting polymer for biomedical applications, Adv. Funct. Mater. 12 (2002) 33–37, https://doi.org/10.1002/1616-3028(20020101)12:1<33::AID-ADFM33>3.0.CO;2-E.
[79] M.C. Vyner, L. Liu, H.D. Sheardown, B.G. Amsden, The effect of elastomer chain flexibility on protein adsorption, Biomaterials 34 (2013) 9287–9294, https://doi.org/10.1016/j.biomaterials.2013.08.086.
[80] J.D. Humphrey, E.R. Dufresne, M.A. Schwartz, Mechanotransduction and extracellular matrix homeostasis, Nat. Rev. Mol. Cell Biol. 15 (2014) 802, https://doi.org/10.1038/nrm3896.
[81] D. Browe, J. Freeman, Optimizing C2C12 myoblast differentiation using polycaprolactone–polypyrrole copolymer scaffolds, J. Biomed. Mater. Res. 107 (2019) 220–231, https://doi.org/10.1002/jbm.a.36556.
[82] K.D. McKeon-Fischer, D.H. Flagg, J.W. Freeman, Coaxial electrospun poly (ε-caprolactone), multiwalled carbon nanotubes, and polyacrylic acid/polyvinyl

alcohol scaffold for skeletal muscle tissue engineering, J. Biomed. Mater. Res. 99A (2011) 493–499, https://doi.org/10.1002/jbm.a.33116.
[83] V.J. Caiozzo, Plasticity of skeletal muscle phenotype: mechanical consequences, Muscle Nerve 26 (2002) 740–768, https://doi.org/10.1002/mus.10271.
[84] R.T. Tran, P. Thevenot, D. Gyawali, J.-C. Chiao, L. Tang, J. Yang, Synthesis and characterization of a biodegradable elastomer featuring a dual crosslinking mechanism, Soft Matter 6 (2010) 2449–2461, https://doi.org/10.1039/C001605E.
[85] Y. Zhang, V. Lukacova, K. Reindl, S. Balaz, Quantitative characterization of binding of small molecules to extracellular matrix, J. Biochem. Biophys. Methods 67 (2006) 107–122, https://doi.org/10.1016/j.jbbm.2006.01.007.
[86] N.T. Kohen, L.E. Little, K.E. Healy, Characterization of Biointerphases Matrigel interfaces during defined human embryonic stem cell culture, Biointerphases 4 (2009) 69–79, https://doi.org/10.1116/1.3274061.
[87] S.S. Soofi, J.A. Last, S.J. Liliensiek, P.F. Nealey, C.J. Murphy, The elastic modulus of Matrigel™ as determined by atomic force microscopy, J. Struct. Biol. 167 (2009) 216–219, https://doi.org/10.1016/j.jsb.2009.05.005.
[88] J. Lee, E. Gazi, J. Dwyer, M.D. Brown, N.W. Clarke, J.M. Nicholson, P. Gardner, Optical artefacts in transflection mode FTIR microspectroscopic images of single cells on a biological support: the effect of back-scattering into collection optics, Analyst 132 (2007) 750–755, https://doi.org/10.1039/B702064C.
[89] A. Bettadapur, G.C. Suh, N.A. Geisse, E.R. Wang, C. Hua, H.A. Huber, A.A. Viscio, J. Y. Kim, J.B. Strickland, M.L. McCain, Prolonged culture of aligned skeletal myotubes on micromolded gelatin hydrogels, Sci. Rep. 6 (2016) 28855, https://doi.org/10.1038/srep28855.
[90] M.-C. Chen, Y.-C. Sun, Y.-H. Chen, Electrically conductive nanofibers with highly oriented structures and their potential application in skeletal muscle tissue engineering, Acta Biomater. 9 (2013) 5562–5572, https://doi.org/10.1016/j.actbio.2012.10.024.
[91] D. Paulin, Z. Li, Desmin: a major intermediate filament protein essential for the structural integrity and function of muscle, Exp. Cell Res. 301 (2004) 1–7, https://doi.org/10.1016/j.yexcr.2004.08.004.
[92] M.L. Costa, R. Escaleira, A. Cataldo, F. Oliveira, C.S. Mermelstein, Desmin: molecular interactions and putative functions of the muscle intermediate filament protein, Braz. J. Med. Biol. Res. 37 (2004) 1819–1830, https://doi.org/10.1590/S0100-879X2004001200007.
[93] P.S. Zammit, Function of the myogenic regulatory factors Myf5, MyoD, Myogenin and MRF4 in skeletal muscle, satellite cells and regenerative myogenesis, Semin. Cell Dev. Biol. 72 (2017) 19–32, https://doi.org/10.1016/j.semcdb.2017.11.011.
[94] H.A. Asfour, M.Z. Allouh, R.S. Said, Myogenic regulatory factors: the orchestrators of myogenesis after 30 years of discovery, Exp. Biol. Med. 243 (2018) 118–128, https://doi.org/10.1177/1535370217749494.
[95] M. Sciancalepore, R. Afzalov, V. Buzzin, M. Jurdana, P. Lorenzon, F. Ruzzier, Intrinsic ionic conductances mediate the spontaneous electrical activity of cultured mouse myotubes, Biochim. Biophys. Acta Biomembr. 1720 (2005) 117–124, https://doi.org/10.1016/j.bbamem.2005.12.001.